DEVELOPMENTAL OSTEOLOGY OF TWO SPECIES OF ECONOMICALLY IMPORTANT SCIAENIDS, *Sciaenops Ocellatus* AND *Cynoscion nebulosus* (TELEOSTEI: SCIAENIDAE)

A Thesis

by

KOLE MATTHEW KUBICEK

Submitted to the Office of Graduate and Professional Studies of
Texas A&M University
in partial fulfillment of the requirements for the degree of

MASTER OF SCIENCE

Chair of Committee,	Kevin W. Conway
Committee Members,	John D. McEachran
	Delbert M. Gatlin III
Head of Department,	Michael P. Masser

May 2014

Major Subject: Wildlife and Fisheries Sciences

ABSTRACT

The red drum (*Sciaenops ocellatus*) and spotted seatrout (*Cynoscion nebulosus*) are two ecomomically important sciaenids currently cultured for stock enhancement in Texas. 237 specimens of *S. ocellatus*, ranging in size from 2.5-26.3mm SL, and 214 specimens of *C. nebulosus*, ranging in size from 2.6-27.7 mm SL, were investigated and utilized to create ossification sequences depicting development of the entire skeleton for both species.

Development of the skeleton, excluding the basisphenoids and sclerotic bones, was complete in *S. ocellatus* and *C. nebulosus* at 14.4 mm SL and 13.5 mm SL, respectively. The basisphenoid did not appear until later in development (21.9 mm SL in *S. ocellatus* and 19.5 mm SL in *C. nebulsosus*), while the sclerotic bones were not present in the material examined. No major differences were identified between the ossification sequences compiled for each species. *Cynoscion nebulosus* exhibited variation in the presence/absence of two elements, supraneural 1 and the coronomeckelian. Development of the skeleton in *S. ocellatus* and *C. nebulosus* was compared with *Agyrosomus meagre* and *Micropogonias furnieri*, two other species of sciaenid for which information on skeletal development is available. No major differences were identified in the development of the axial skeleton between *A. meagre*, *S. ocellatus* or *C. nebulosus*. Several notable differences were identified in the development of the neurcranium between *M. furnieri* and that of *S. ocellatus* and *C. nebulosus*, suggesting that variation may exist in the development of the neurocranium across Sciaenidae. Lastly, the ossification sequence compiled here for *S. ocellatus* was compared to that of *Danio rerio*, the only other species of teleost for which an ossification sequence is available for development of the entire skeleton, and *Chanos chanos*, for which an ossification sequence is available for the cranial skeleton. Several differences were identified between all three species, suggesting variation of skeletal development exists across Teleostei. The information provided herein will benefit the culture of *S. ocellatus* and *C. nebulosus* by providing information on normal skeletal

development and a standard reference sequence of skeletal development for both species that will facilitate identification of skeletal malformations should they become an issue in the future.

DEDICATION

I dedicate this thesis in memory of my nephew, Hayden Riley Beeson.

ACKNOWLEDGEMENTS

I would like to thank my committee chair, Dr. Kevin W. Conway, for guidance as well as introducing me to the fascinating world of fish bones. I also thank my committee members, Dr. John McEachran and Dr. Delbert Gatlin III for their helpful advice and comments. Thanks also go to the Staff of the Texas Parks and Wildlife Department's Marine Hatchery at Sea Center Texas (Lake Jackson, Tx), including David Abrego, Shane Bonnot, Courtney Moore, Jeff Bayer and Jennifer Butler, for their help and patience during the collection of the specimens used in this study. Funding for this research was provided by Texas A&M Agrilife Research, Texas Sea Grants grants in aid of graduate research and Texas A&M/CONACYT Collaborative Research Grant Program. Finally, thanks to my family and friends for all of their support as well as my girlfriend Katie Ondrias, for motivating me to further my education.

TABLE OF CONTENTS

LIST OF FIGURES

INTRODUCTION

The Family Sciaenidae is a diverse group of perciform fishes (Order Perciformes) that contains approximately 70 genera and 275 species (Nelson, 2006). Commonly referred to as drums, croakers, and weakfishes, several species of sciaenid are economically important, being highly valued either for commercial or recreational purposes (Neira et al., 1998). As such, sciaenids have been the subject of intense scientific inquiry, with topics ranging from physiology and nutrition (Daniel, 2004; Li et al., 2005; Ono & Poss, 1982; Ramcharitar et al., 2006) to ecology and life history (Acha et al., 1999; Blasina et al., 2010; Thomas, 1971). Several studies have investigated the anatomy of sciaenid fishes, with the majority focused on the complex morphology of the swim bladder and associated musculature (Ono & Poss, 1982), which is involved in sound production (Ramcharitar et al., 2006). Several authors have also attempted to further our understanding of sciaenid phylogenetic relationships through comparative investigations of the musculoskeletal system (Green, 1941; Sasaki, 1989; Taniguchi, 1969a, 1969b, 1970; Topp & Cole, 1968).

Despite the vast wealth of information available on adult morphology, information on early development of sciaenids is scarce, perhaps due to the difficulty of obtaining early developmental stages. Of the ontogenetic studies available for sciaenids, the majority have focused almost exclusively on external characteristics, such as larval pigmentation (Fruge & Truesdale, 1978; Holt et al., 1981) or fin development (Kengo Itagaki et al., 2007). To date, relatively few studies have investigated aspects of early skeletal ontogeny in sciaenids in detail (Jardim and Santos, 1994; Cardiera et al., 2012). Studying skeletal ontogeny can lead to a better understanding of adult morphology and can also contribute novel morphological information for phylogenetic investigations (Britz and Johnson, 2002, 2005, 2012). Additionally, it can provide a standard reference of osteological development for cultured species, where skeletal malformations are of major concern (Koumoundouros et al., 1997; Gavaia et al., 2002; Tong et al., 2012).

The economically important red drum (*Sciaenops ocellatus*) and spotted seatrout (*Cynoscion nebulosus*) represent excellent candidate species for expanding our understanding of the sciaenid skeletal system and its development. Both species are currently produced as part of a stock enhancement program in the state of Texas. The program was initiated after natural populations had reached all-time lows and now several million *S. ocellatus* fingerlings and approximately one million *C. nebulosus* fingerlings are released every year into Texas bays and estuaries (Vega et al., 2009). Although stock enhancement efforts for both species are highly successful, skeletal malformations are caused by a variety of factors that all cultured species can be subjected to (Gavaia et al., 2002; Koumoundouros, 2010). For this reason, it is important to understand the skeletal development of *S. ocellatus* and *C. nebulosus*, especially since both are currently used to supplement wild populations. The style and formatting for this paper are based on the guidlines of the journal of applied ichthyology.

The major goal of this study is to advance understanding of early skeletal development in sciaenid fishes by: (1) developing a high quality photographic atlas of skeletal development for *S. ocellatus;* and (2) determining the sequence of ossification for the entire skeleton in both *S. ocellatus* and *C. nebulosus*.

MATERIALS AND METHODS

Specimens of *Sciaenops ocellatus* and *Cynoscion nebulosus* were collected from the Texas Parks and Wildlife Department Sea Center Texas Hatchery (Lake Jackson, TX). Approximately 10-15 specimens of each species were sampled daily from the same spawning batch from one day post hatch (dph) up to 30 dph. Once collected, specimens were euthanized through administration of an overdose treatment of Tricaine methanesulfonate (MS-222) and fixed in a solution of 10% buffered formalin for 24 hours. Larvae were then transferred through a series of graded ETOH solutions (30%, 50%) for 24 hours each before final storage in a 70% ETOH solution. A total of 145 *S. ocellatus* and 133 *C. nebulosus*, ranging in size from 2.5-26.3 mm (notochord length [nl] for preflexion larvae/standard length [sl] for postflexion larvae) and 2.6-27.3 mm nl/sl, respectively, were cleared and double stained for bone and cartilage investigation following the method of Taylor and van Dyke (1985). Once cleared and double stained, specimens were then dissected following the protocol of Weitzman (1974) and scored for the presence/absence of 149 skeletal elements under a ZEISS SteREO Discovery V20 stereomicroscope. For each individual specimen, bones were considered present at the first sign of alizarin red S staining and absent in the absence of alizarin red S staining. In the few cases in which it was not possible to confirm through stereomicroscopy whether a particular bone was ossified, specimens were examined at higher magnification under transmitted light using a ZEISS Primo Star compound microscope. The clearing and double staining protocol of Taylor & van Dyke (1985) relies on an acidic solution for cartilage staining that has been reported previously to negatively affect the staining of bone (Walker and Kimmel, 2007), which could hamper the identification of bony elements, particularly during the earliest stages of ossification. In order to compensate for this, a smaller number of specimens of each species (92 *S. ocellatus* and 81 *C. nebulosus)* were cleared and single stained with alizarin red S for bone investigation following the protocol modified from Taylor (1967) and scored for the presence/absence of bone. In this case, data collected from double or single stained specimens were highly congruent and were combined. After data collection, Microsoft

Excel© was used to compile bone presence/absence data and identify the smallest size at which a particular ossification was present. These data were utilized to compile a sequence of ossification for each species using the general protocol of Cubbage and Mabee (1996) and Bird and Mabee (2003) to document the progression of skeletal development from the earliest stages through to completion. Lastly, selected individuals (and dissected parts thereof) were photographed using a ZEISS Axiocam MRc5 digital camera attached to a ZEISS SteReo Discovery V20 stereomicroscope. Images were processed using Abode Photoshop CS5.1 and Illustrator CS5.1. All material examined has been deposited in the Collection of Fishes at the Biodiversity Research and Teaching Collections (BRTC) of Texas A&M University (*S. ocellatus*, TCWC 16420.01 & TCWC 16421.01; *C. nebulosus*, TCWC 16422.01 & TCWC 16423.01).

RESULTS

Neurocranium

I describe five different stages in the development of the neurocranium. The sequence of ossification for this region is: parasphenoid (3.1 mm NL); basioccipital, exoccipital, frontal (4.4. mm NL); prootic (4.5 mm NL); supraoccipital, vomer, autopterotic (4.8 mm NL); epioccipital (5.2 mm SL); autosphenotic (5.3 mm SL); intercalar (6.0 mm SL); nasal (6.4 mm SL); ethmoid (7.8 mm SL); parietal (7.9 mm SL); lateral ethmoid (8.3 mm SL); dermopterotic (8.9 mm SL); pterosphenoid (10.0 mm SL); dermospenotic (10.6 mm SL); medial extrascapular, lateral extrascapular (11.4 mm SL); and basisphenoid (21.9 mm SL).

In the smallest stage illustrated (4.1 mm NL; Figure 1A), the chondrocrainium is well developed and there are only four ossifications present. In the orbital region, the frontal is present as a domed lamina of dermal bone, situated dorsal to the taenia marginalis posterior. The frontal also dorsally overlaps the lateral edge of the epiphyseal bar, with the majority of the bone situated posterior to this element. The thin dermal parasphenoid is located centrally along the ventral surface of the chondrocranium, between the medial edges of the parachordal cartilages. Anteriorly, the parasphenoid terminates in a sharp point and rests ventral to the trabeculae that form the trabecula communalis. In the occipital region the perichordally ossified basioccipital is present as a cap of bone around the anterior end of the notochord, with its anteriormost tip situated dorsal to the posteriormost tip of the parasphenoid. The exocipital is represented at this stage only by a small endochondrally ossified rim of bone around the posteroventral margin of the occipital arch.

At 6.7 mm SL (Figure 1B), the neurocranium is still largely comprised of chondrocranium. The vomer is now present as a sliver of dermal bone, ventral to and extending the entire width of, the anterior edge of the ethmoid plate. The nasal (not illustrated) is also now present as a thin concave gutter-like dermal ossification, situated

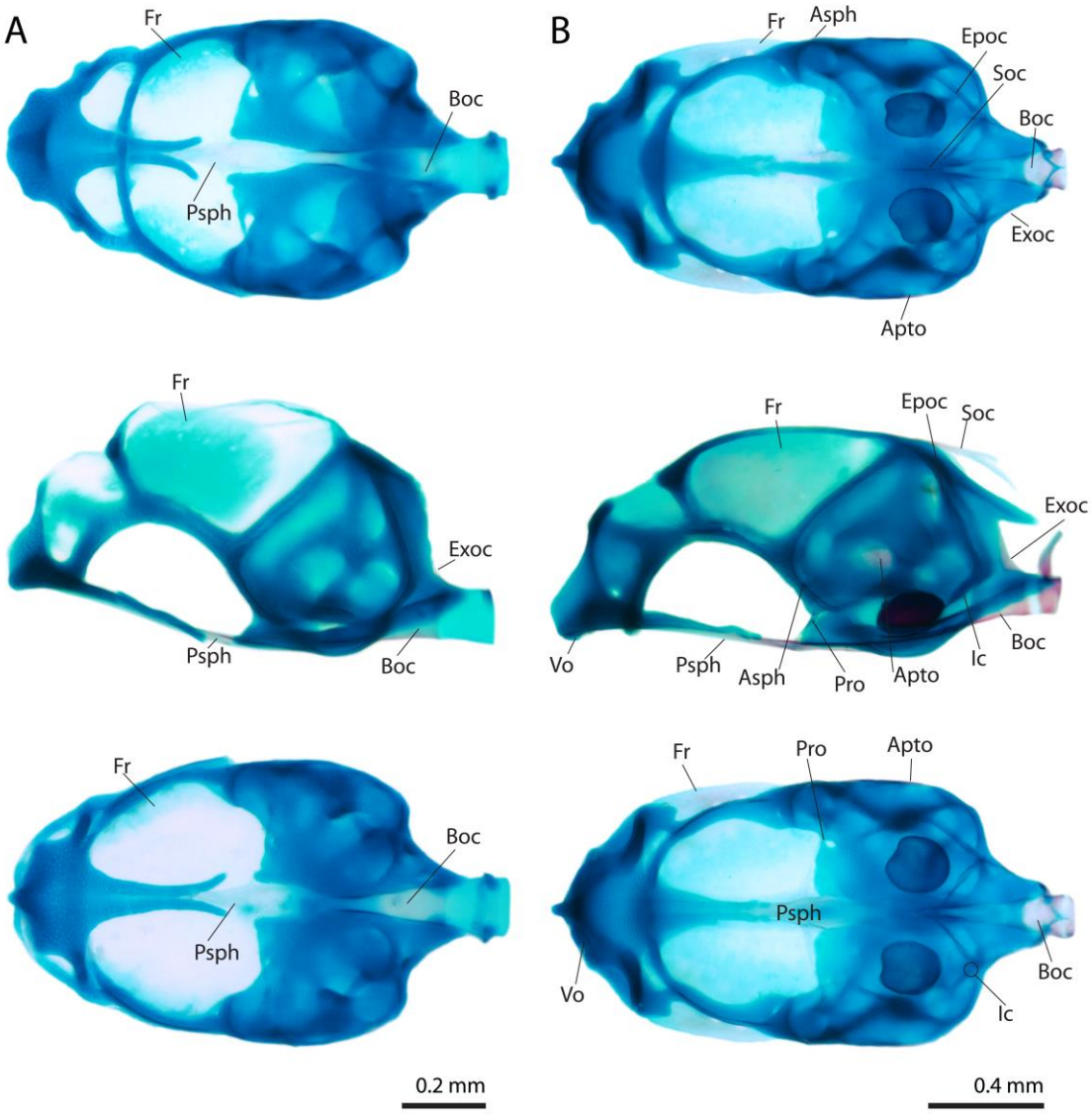

Fig. 1. Ontogeny of the neurocranium of *S. ocellatus* (TCWC 16420.01) in dorsal, lateral and ventral view. Nasals and Extrascapulars not illustrated. **A.** 4.1 mm NL. **B.** 6.7 mm SL. **C.** 9.5 mm SL. **D.** 12.9 mm SL. **E.** 25.3 mm SL. Apto, Autopterotic; Asph, Autosphenotic; Boc, Basioccipital; Bsph, Basisphenoid; Dpto, Dermopterotic; Dsph, Dermosphenotic; E, Ethmoid; Epoc, Epioccipital; Exoc, Exoccipital;Fr, Frontal; Ic, Intercalar; LE, Lateral Ethmoid; Pa, Parietal; Pro, Prootic; Psph, Parasphenoid; Pto, Pterotic; Ptsph, Pterosphenoid; Sag, Sagitta; Soc, Supraoccipital; Sph, Sphenotic; Vo, Vomer.

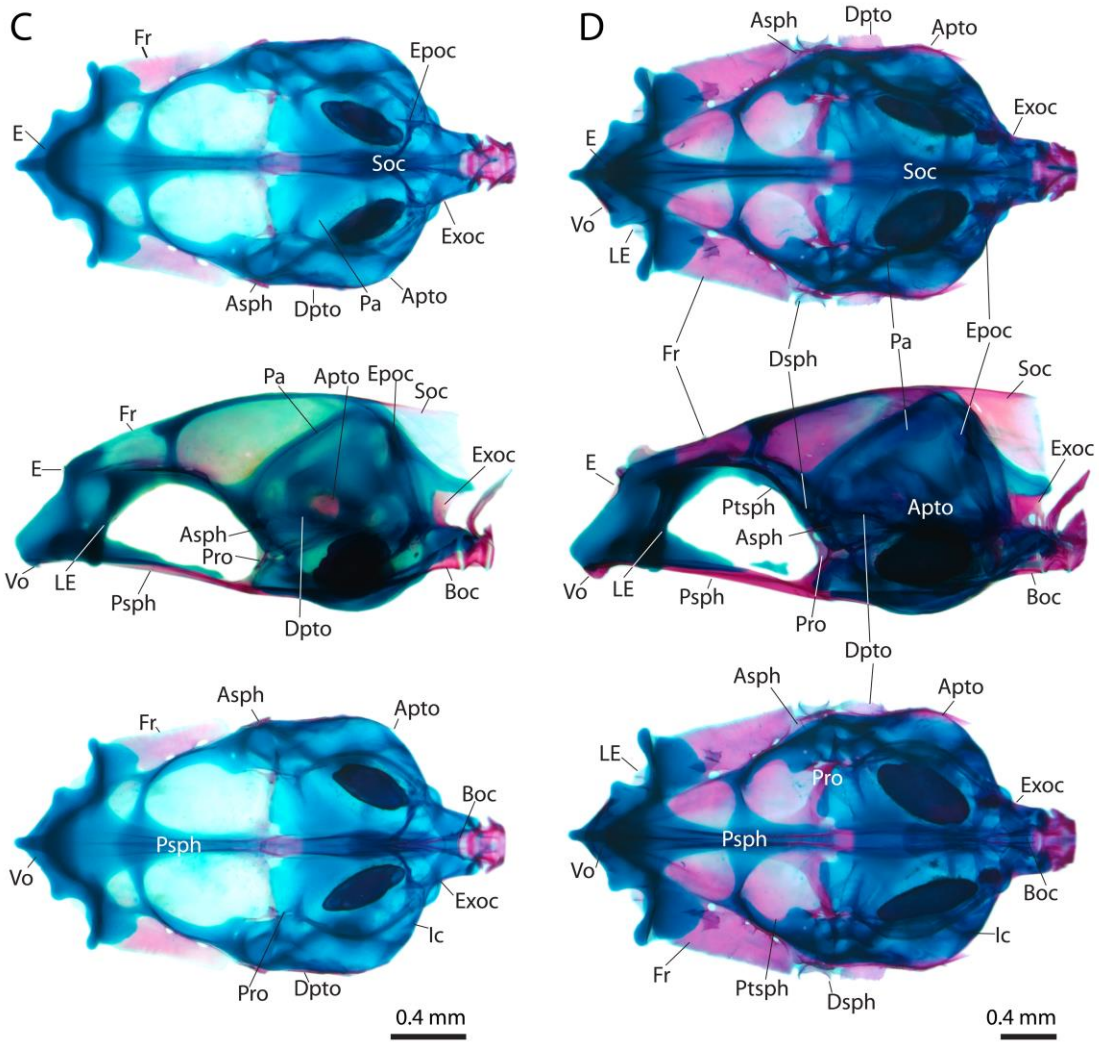

Fig.1 Continued

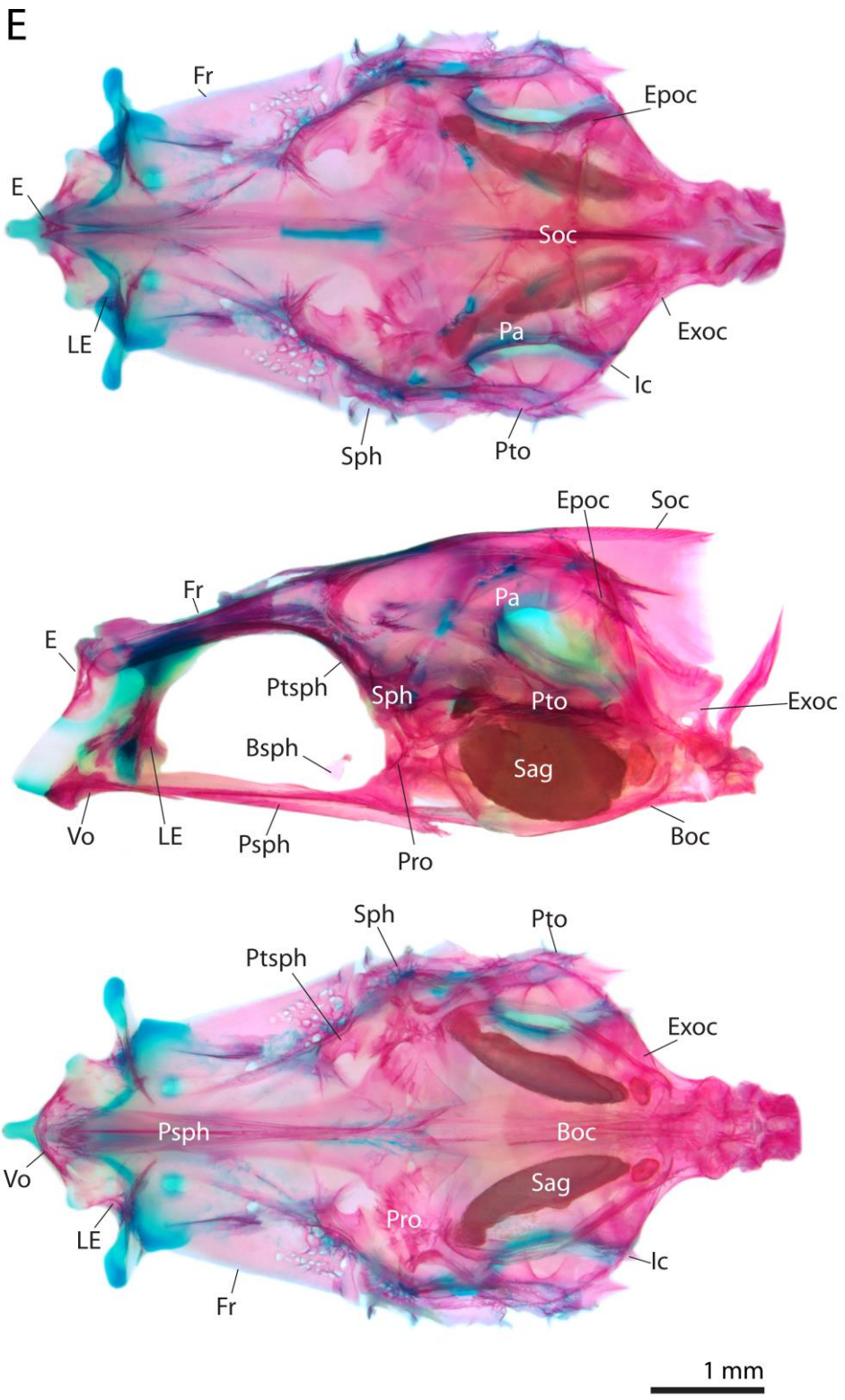

Fig. 1 Continued

anterior to the lateral edge of the frontal. The frontal now covers most of the dorsal surface of the chondrocranium, from the posterior margin of the ethmoid plate to the anterodorsal edge of the otic capsule. Both frontals meet along the dorsal midline anteriorly, however, they have yet to meet posteriorly, leaving the posterior half of the taenia tecti medialis uncovered. A shallow groove is now present along the lateral edge of the frontal, opposite the taenia marginalis posterior, forming the supraorbital ridge in which pits associated with neuromast formation in the frontal portion of the supraorbital sensory canal are now present. The parasphenoid now rims the entire ventral surface of the trabecula communalis and partially overlaps the posteroventral edge of the ethmoid plate. Short dorsolateral wings are now present along the lateral margins of the parasphenoid, situated just anterior to the floor of the otic region. In the otic region the prootic is ossified both perichondrally and endochondrally around the anterolateral arm as well as perichondrally along its anteromedial edge. The autosphenotic is now present as a thin perichondrally ossified lamina of bone midway along the anterolateral edge of the otic capsule. Posterior to the autosphenotic, the autopterotic is present as a thin plate of perichondrally ossified bone around the lateral semicircular canal. The intercalar is present on the posterior surface of the otic capsule as a tiny ossification that is connected to the ventral process of the posttemporal via a short ligament. All four bones of the occipital region are now present. The supraoccipital is represented by a thin perichondrally ossified lamina of bone that caps the posterodorsalmost point of the otic capsule. A well-developed crest of membrane bone is present along the midline of the supraoccipital that extends posterior to the otic capsule and dorsal to the tectum synoticum. The epioccipital is now present as a small endochondrally ossified bone, on the posterolateral edge of the otic capsule, which articulates directly with the dorsal process of the posttemporal. The exocipital has expanded considerably and now rims much of the occipital arch and has also started to ossify perichondrally around the margin of the foramen for the Vagus (X) nerve. The perichordrally ossified core of the basioccipital is now also surrounded by perichondral ossification.

At 9.5 mm SL (Figure 1C), large cartilaginous expanses of the chondrocranium persist, however, almost all of the endoskeletal bones are now present and ossified endochondrally. The ethmoid is now present and represented by a thin lamina of perichondrally ossified bone over the anterodorsal surface of the ethmoid plate that exhibits two small flanges of bone. The lateral ethmoid now present and ossified perichondrally around the midlength of the lamina orbitonasalis. The vomer has grown in size but retains a similar shape to that described in the previous stage. The lateral edges of the nasal now extend dorsally to rim the lateral margin of the nasal portion of the supraorbital sensory canal. The frontal now completely covers the dorsal surface of the anterior half of the neurocranium and now contacts the anterior margin of the supraoccipital posteromedially. The supraorbital ridge along the lateral edge of the frontal has also expanded and now covers the dorsal surface of the lamina orbitonasalis. The lateral edges of the parasphenoid now possess ventral keels, which run much of the length of the bone. The lateral arms of the parasphenoid are now sutured to the anterolateral margin of the prootics. The prootic has further ossified endochondrally around the trigomenisfacialis canal located anteriorly in the floor of the otic capsule and several ridges of membrane bone are also now present along the perichondrally ossified component of the prootic. The parietal is now present as a thin dermal ossification along the anterodorsal edge of the otic capsule. The mostly perichondrally ossified autosphenotic now possesses a projection of membrane bone that extends ventrolaterally from the center of its lateral face. The autopterotic has expanded further posteriorly and now exhibits a small spine-like extension posterolaterally. The dermopterotic is also now present as thin sliver of dermal bone extending along the base of the otic sensory canal adjacent to the autopterotic. The intercalar has continued to grow and now extends medially and has ossified endochondrally around the anterodorsal edge of the fossa located along the anterior edge of exoccipital. The supraoccipital is now also ossified endochondrally around the base of the supraoccipital crest and now also incorporates the posterior region of the taenia tecti medialis, where it meets the frontal anteriorly. The supraocciptial crest has grown posteriorly and ventrally to meet the dorsal edge of the

tectum synoticum forming a plate of membrane bone. The epioccipital now exhibits a well-developed ridge of membrane bone that extends posterodorsally from the surface of the bone. The exoccipital has expanded both posteriorly, to meet the ventral edge of the tectum synoticum forming the roof of the foramen magnum along with the first vertebral centrum via the exoccipital condyles, and anteriorly, within the posterolateral margin of the otic capsule, to meet the intercalar laterally and the basioccipital ventromedially. The basioccipital now possesses two well-developed ridges of membrane bone along its posteroventral surface and the cartilage of the floor of the otic capsule lateral to the perichordally ossified component of the basioccipital has now ossified endochondrally.

At 12.9 mm SL (Figure 1D), all bony elements of the neurocranium are now present except for the basisphenoid. The ethmoid has expanded considerably and is now also ossified endochondrally along the dorsomedial surface of the ethmoid plate. In addition to the plate of bone surrounding the mid-region of the lamina orbitonasalis, the lateral ethmoid has also now ossified perichondrally around the two facets present ventrally on the lamina orbitonasalis. The vomer now covers much of the ventral surface of the ethmoid plate. The nasal has retained a similar shape to that described for previous stages but is now much larger and separated from the anterior edge of the frontal only by short gap. The frontal now exhibits several bony protrusions, representing the first signs of bony struts that will later roof the supraorbital sensory canal. The supraorbital ridge along the lateral edge of the frontal now contacts the autosphenotic posteriorly and has further expanded anteriorly, past the anterior margin of the lamina orbitonasalis. Minor surface sculpturing is also now present over the surface of the frontal, especially along the trench of the supraorbital ridge. The pterosphenoid has begun to ossify perichondrally around the inner edge of the taenia marginalis posterior. The anteriormost tip of the parasphenoid now lies dorsal to the vomer and ventral to the ethmoid plate. Posteriorly, the parasphenoid is now also in direct contact with the basioccipital. Dorsal to the parasphenoid, the posteriormost tip of the traebecula communis has become separated from the rest of the cartilage. The prootic is now well ossified endochondrally along its anterior edge but remains only weakly perichondrally ossified posteriorly,

particularly around the anterior margin of the lagenar capsule to which to prootic contributes. The parietals have grown considerably and now extend from the anterodorsal margin of the autopterotic to the anterior margin of the epiocipital. The autosphenotic is now almost entirely perichondrally ossified and the dermosphenotic is now present as a small concave dermal ossification adjacent to the lateral flange of membrane bone borne on the lateral face of the autosphenotic. The autopterotic is now also completely perichondrally ossified and the spine-like process along the lateral edge is now obvious in both dorsal and lateral views. The dermopterotic has expanded laterally into a thin lamina of bone just posterior to the dermosphenotic. The intercalar has also expanded and now rims the posterior margin of the autopterotic dorsally. The lateral and medial extrascapulars (not illustrated) are now present as thin lamina of dermal bone on the lateral surface of the otic capsule between the autopterotic and the epioccipital and provide support to the otic and supratemporal sensory canals, respectively. The supraoccipital has extended anteriorly to a point dorsal to the center of the taenia tecti medialis. The supraoccipital crest has also continued to grow but has changed little in shape from that described for the previous stage. The epioccipital is now endochondrally ossified and the flange of membrane bone has widened and extended further posteriorly, beyond the posterior margin of the otic capsule. The exoccipital has expanded to border the entire lateral margin of the foramen magnum. The basioccipital has continued to expand laterally but remains similar in overall appearance to that described for the previous stage.

In the final stage illustrated (25.3 mm SL, Figure 1E), representing the adult condition, most of the chondrocranium has been replaced by endochondral bone or surrounded by dermal bone. The flanges of membrane bone on the dorsal surface of the ethmoid are now sutured posteriorly with the anterior edge of the frontal. A well-developed median ridge of membrane bone is also now present along the anterior edge of the ethmoid, extending along the upper part of the nasal septum of the ethmoid plate. Much of the lamina orbitonasalis has now been replaced by the lateral ethmoid, with cartilage remaining only at the lateralmost tip of the ectethmoid process and around the former

junction of the lamina orbitonasalis and the taenia marginalis anterior. The vomer now tapers to a point posteriorly to cover the anterior portion of the parasphenoid ventrally and exhibits dorsolateral extensions, which extend dorsally to contact the cartilage remaining within the rostropalatine facet of the lamina orbitonasalis. Extensive sculpturing is also now present over the anteroventral surface of the vomer. The nasal is now much larger and exhibit extensive sculpturing anteriorly. The anterior edge of the nasal now contacts the dorsal edge of infraorbital one. The bony protrusions located on the dorsal surface of the frontal have continued to expand to further enclose the supraorbital sensory canal. The sculpturing over the dorsal surface of the frontal is now more extensive, especially around the base of the bony processes supporting the supraorbital sensory canal and the surface of the orbital ridge. The pterosphenoid is now well ossified endochondrally and is separated from the prootic posteroventrally by a small strip of cartilage (a remnant of the taenia marginalis posterior) and makes direct bony contacts with the sphenotic posterodorsally and the frontal dorsally. The basisphenoid (the last bone to develop in the neurocranium) is now ossified endochondrally within the small remnant of trabecular communalis cartilage dorsal to the parasphenoid. The parasphenoid is now sutured posteriorly to the basisphenoid and possesses a well-developed ventral keel that stretches along the ventral surface from a point slightly posterior to the vomer to a point slightly anterior to the posterior edge of the prootic. The prootic is now completely ossified and possesses sculpturing around the struts of bone surrounding the openings for the trigeminofacialis. The posterior edge of the prootic contributes to the anterolateral margin of the lagenar capsule (otic bulla) where it is separated from the basioccipital and exoccipital by a wide strip of cartilage (a remnant of the floor of the otic capsule). The parietal is now sutured to the epioccipital posteriorly and the autosphenotic anterolaterally. It is bordered anteromedially by the frontal and posteromedially by the supraoccipital. The dermosphenotic and autosphenotic are now fused (ontogenetically) to form the spenotic. The dermopterotic and autopterotic are also now fused (ontogenetically) to form the pterotic. The lateral extensions along the surface of the former dermopterotic have extended dorsally to

partially enclose the otic sensory canal. The intercalar now possess a well-developed central depression where it accomodates the ventral process of the posttemporal. The lateral extrascapular is now more heavily ossified and is now bifurcated anteriorly into a dorsal and anterior canal. The anterior canal connects with the otic sensory canal as it leaves the posterior margin of the pteroric, while the dorsal canal connects with supratemporal canal via the medial extrascapular. The medial extrascapular now rests dorsal to the epioccipital, just posterior to the parietal and supports the supratemporal sensory canal. The supraoccipital crest has expanded significantly and there are now two posteriorly directed ridges of bone located midway along its lateral surface. The epioccipital is now separated from the supraocciptial by only a thin sliver of cartilage and the posterodorsal extension has expanded to better accommodate the dorsal arm of the posttemporal. The exoccipital is now strongly sutured to the supraoccipital dorsally and a foramen is now present in the lateral wall of the exoccipital dorsal to the exoccipital condyle. The basioccipital is now completely ossified endochondrally and contributes to the posteromedial margin of the lagenar capsule (otic bulla) on the ventral surface of the otic capsule.

Comparison to C. nebulosus

The sequence of ossification for this region in *C. nebulosus* is: parasphenoid (3.3 mm NL); frontal (3.5 mm NL); basiocciptial, exoccipital (3.6 mm NL); prootic (3.8 mm NL); supraoccipital (4.4 mm NL); vomer, autopterotic (4.7 mm NL); autosphenotic (5.0 mm SL); epiocciptial (5.3 mm SL); intercalar (5.5 mm SL); nasal (5.9 mm SL); ethmoid (6.6. mm SL); lateral ethmoid (8.0 mm SL); parietal (8.5 mm SL); dermopterotic (9.3 mm SL); pterosphenoid (10.0 mm SL); lateral extrascapular, medial extrascapular (11.8 mm SL); dermosphenotic (12.0 mm SL) and basisphenoid(19.5 mm SL).

The sequence of ossification for this region in *C. nebulosus* differed slightly from that of *S. ocellatus*. In *C. nebulosus*, the frontal develops earlier than the basioccipital and the exoccipital (compared to developing at the same time in *S. ocellatus*), the autosphenotic develops earlier than the epioccipital, and the lateral ethmoid develops earlier than the

parietal. The dermosphenotic also develops later in the *C. nebulosus,* after the extrascapulars (compared to earlier than the extrascapulars in *S. ocellatus*). The adult neurocranium of *C. nebulosus* is similar to that of *S. ocellatus*, differing only in overall shape (appearing more shallow and elongated in *C. nebulosus*) and the shape of individual bones, specifically the membrane bone flange of the epiocipital, which is greatly elongated in *C. nebulosus*, extending well beyond the posterior edge of the neurocranium.

Hyopalatine Arch and Opercular Series

I describe six different stages in the development of the suspensorium (including elements of the hyopalatine arch, jaws and opercular series). The sequence of ossification for this region is: maxilla (2.5 mm NL); dentary, opercle and premaxilla (3.1 mm NL); anguloarticular (3.6 mm NL); symplectic (3.7 mm NL); endopterygoid and quadrate (3.9 mm NL); subopercle (4.2 mm NL); preopercle (4.3 mm NL); hyomandibular, retroarticular and ectopterygoid (4.4. mm NL); interopercle (4.7 mm NL); autopalatine (5 mm SL); metapterygoid (5.3 mm SL) and coronomecklian (6.3 mm SL).

In the smallest stage illustrated (3.6mm NL; Figure 2A), the hyopalatine arch is predominately cartilage, with a few poorly developed dermal ossifications. The hyosymplectic cartilage is well developed with the pars symplectica situated along the ventral margin of the quadratometapterygoid portion of the palatoquadrate cartilage. No ossifications are present in the hyosymplectic or palatoquadrate cartilages at this stage. The endopterygoid is present as a thin sliver of dermal bone, situated dorsal to the pars autopalatina. The pars quadrata articulates anteroventrally with the posterodorsal tip of Meckel's cartilage to form the quadrato-mandibular joint. Of the two lower jaw bones present, the dentary is already well developed and extends from the anterior of Meckel's cartilage posteriorly until it contacts the compound anguloarticular, the result of earlier ontogenetic fusion between the dermal angular and endoskeletal articular. The anguloarticular extends from below a short anterodorsally directed projection of

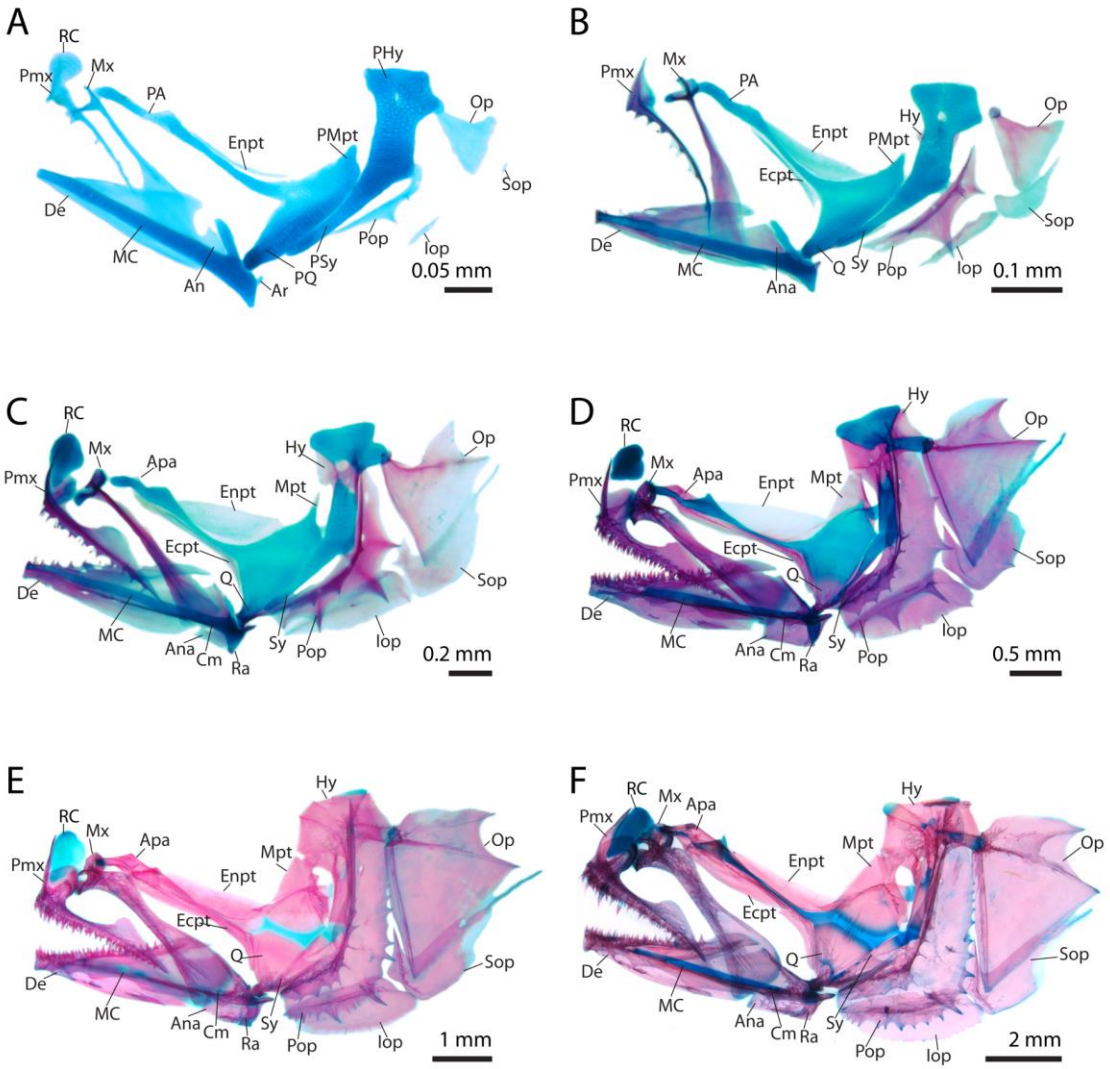

Fig. 2. Ontogeny of the hyopalatine arch, jaws, and opercular series of *S. ocellatus* (A-E, TCWC 16420.01; F TCWC 12308.24). **A.** 3.6 mm NL. **B.** Rostral cartilage not shown, 4.1 mm NL. **C.** 6.7 mm SL. **D.** 12.9 mm SL. **E.** 25.3 mm SL. **F.** 43.2 mm SL. An, Angular; Ana, Anguloarticular; Apa, Autopalatine; Ar, Articular; Cm, Coronomeckelian; De, Dentary; Ecpt, Ectopterygoid; Enpt, Endopterygoid; Hy, Hyomandibular; Iop, Iteropercle; MC, Meckle's Cartilage; Mpt, Metapterygoid; Mx, Maxilla; Op, Opercle; PA, Pars Autopalatina; PHy, Pars Hyomandibula; PMpt, Pars Metapterygoidea; Pmx, Premaxilla; Pop, Preopercle; PQ, Pars Quadrata; PSy, Pars Symplectica; Q, Quadrate; Ra, Retroarticular; RC, Rostral Cartilage; Sop, Subopercle; Sy, Symplectic.

Meckel's cartilage and terminates as a tiny rounded process ventral to the quadrato-mandibular joint. Both of the upper jaw bones are present and well developed. The

premaxilla is a thin dermal bone with a short ascending process that articulates with the anterior edge of the rostral cartilage. The premaxilla extends posteroventrally to the dorsal margin of the dentary and already excludes the maxilla from the gape. At this stage, three small coniform teeth are present along the ventral surface of the premaxilla. The maxilla is a thin dermal bone that is bifurcated anteriorly into dorsal and ventral rami. The ventral ramus extends anteroventrally towards the premaxilla, while the dorsal ramus extends dorsally towards the anteriormost tip of the pars autopalatina. The flattened posteroventral region of the maxilla rests along the lateral edge of the dentary. All four bones of the opercle series are present and represented by poorly ossified lamina or dermal bone. The opercle articulates with the posterior most edge of the pars hyomandibular of the hyosymplectic cartilage. It has already taken on its shield-like shape. The preopercle has two spines present posteriorly and rests along the ventral edge of the pars symplectica of the hyosymplectic cartilage. Both subopercle and interopercle are represented by tiny splint-like bones, situated posteroventrally to the opercle and preopercle, respectively.

At 4.1 mm SL (Figure 2B), the hyomandibular has begun to ossify perichondrally within the pars hyomandibula, just ventral to the foramen for the passage of the facial portion of the trigeminal nerve located on the dorsal head of the hyosymplectic cartilage. Two small flanges of membrane bone, one anterior and one posterior, flank the shaft of the pars hyomandibula, adjacent to the perichondrally ossified region at its center. The symplectic is also present and has begun to ossify perichondrally around the anterior tip of the pars symplectica. The quadrate has begun to ossify perichondrally around the pars quadrata at its point of articulation with the lower jaw. The endopterygoid has expanded posterodorsally into a thin lamina of bone and the ectopterygoid is now present as a thin slither of dermal bone ventral to the pars autopalatina. The anterior region of the anguloarticular now extends forward across the posterior margin of the dentary, on which a small posterodorsally directed coronoid process is now present. Small coniform teeth are also present on the dentary, close to the symphysis of the lower jaw. The ascending process of the premaxilla has developed a rounded lamina of bone at its base,

which cups the entire anterior margin of the rostral cartilage. The ventral portion of this lamina extends towards the ventral ramus of the maxilla. The maxilla has continued to widen ventrally to dorsally and there is now a third dorsomedial ramus, which extends posterodorsally from the posteromedial tip of the maxilla to make contact with the anterior tip of the pars autopalatina. The opercle and interopercle are similar in shape to that described in the previous stage but are now much larger. The preopercle has grown considerably and now extends between the symplectic to the membrane bone flange on the posterior edge of the hyomandibular. A well-ossified ridge of bone, with a secondary set of spines, is now present along the dorsal edge of the preopercle and small pits, associated with neuromast formation in the preopercular portion of the preopercular-mandibular sensory canal, are present in the shallow trough formed between the dorsal ridge and main shaft of the bone. The subopercle is now much larger and is slightly curved dorsoventrally, terminating in a thin posterodorsally directed tip.

At 6.7 mm SL (Figure 2C), the hyomandibular is now completely ossified and has replaced the cartilage between the dorsal head and ventral arm of the pars hyomandibula. The flange of membrane bone along the anterior edge of the hyomandibular has expanded considerably anteriorly, whereas the posterior flange of membrane bone has expanded ventrally to flank the posterodorsal edge of the pars hyomandibula. The symplectic has also continued to ossify in a dorsal direction and is now more tightly associated with the posterior edge of the quadratometapterygoid portion of the palatoquadrate cartilage. The ventral region of the quadrate is almost completely ossified and the metapterygoid has begun to ossify perichondrally around the dorsal extension of the pars metapterygoidea, which is capped dorsally by a thin extension of membrane bone. The autopalatine has also started to ossify within the anterior portion of the pars autopalatina and is in contact with the anterior tip of the ectopterygoid, which now extends along most of the anterior edge of the palatoquadrate cartilage, from the autopalatine to the anterodorsal margin of the quadrate. The endopterygoid is now much wider but still retains a similar shape. On the lower jaw the posteroventral most tip of Meckel’s cartilage is surrounded by the perichondrally ossified retroarticular and the

coronomoceklian is now present as a tiny ossification on the posteromedial face of Meckel's cartilage. The coronoid process of the dentary now extends almost to the dorsalmost point of the anguloarticular. Small pits associated with neuromast formation in the mandibular portion of the preopercular-mandibular canal are now clearly visible on both the dentary and anguloarticular. The ascending process of the premaxilla is now much larger, with the posterior extension now in direct contact with the ventral ramus of the maxilla. A thin lamina of bone is now present along the dorsal edge of the posterior half of the premaxilla. The maxilla has continued to widen along its entire length and the dorsal and dorsomedial rami are now joined by a thin lamina of bone. The opercle now possesses three spine-like projections along its posterior margin, with well-ossified ridges extending between the articular head and the tips of the two lowermost projections. The preopercle now extends along the entire ventral margin of the hyosymplectic cartilage ventral to its dorsal head and possesses more spines along both the dorsal ridge and the ventral margin of the bone. The subopercle is much larger with its dorsal edge now articulating with the ventral edge of the opercle and its anterior edge articulating with the posterior tip of the interopercle. The interopercle now terminates in a spine-like projection anteriorly, which accommodates the posterior tip of the retroarticular ligament, and is partially covered by two well-developed spines along the ventral edge of the preopercle.

At 12.9 mm SL (Figure 2D), much of the dorsal head of the pars hyomandibula is now completely ossified perichondrally. The entire anterior portion of the pars symplectica is now surrounded by the perichondrally ossified symplectic, which has developed low flanges of membrane bone along its dorsal and ventral margins. The quadrate and the metapterygoid have now replaced almost the entire quadratometapterygoid portion of the palatoquadrate cartilage. The autopalatine has also increased in size, with well-developed flanges of membrane bone now extending along the dorsal and ventral edge of the pars autopalatina. The endopterygoid and the ectopterygoid have continued to increase in size but have changed little in shape compared to that described for earlier stages. The coronmecklian is larger and has attained a triangular shape. The

retroarticular now borders the entire posteroventral edge of the anguloarticular. The short anterodorsal projection of cartilage on the posterior end of Meckel's cartilage has almost completely ossified endochondrally as part of the anguloarticular. Bony ridges have begun to form along the lateral edge of the dentary, representing the early signs of a bony canal around the preopercle-mandibular sensory canal. Several rows of small coniform teeth, with slightly recurved tips, are present along the dentary and premaxilla. The acrodine caps of several replacement teeth are visible in low crypts along the labial edge of both the dentary and premaxilla (i.e., tooth replacement is intraosseus labially). The ascending process of the premaxilla is now much larger and the articulation between the posterodorsal tip of the premaxilla and the ventral ramus of the maxilla is strongly developed, as is the articulation between the posterodorsal tip of the maxilla and the anterior tip of the autopalatine. The posteroventral shaft of the maxilla now rests along the lateral face of the well-developed coronoid process of the dentary, with its posteriormost tip positioned lateral to the junction between the dentary and anguloarticular. The mid-section of the maxilla is in direct contact with the crest along the dorsal edge of the posterior half of the premaxilla. Spines are now present on all bones of the opercular series. The subopercle now exhibits a well-developed anterodorsally directed process anteriorly. The thin posterior projection of the subopercle has extended considerably and now accounts for half of the total length of the bone.

At 25.3 mm SL (Figure 2E), the hyomandibular is now completely ossified, except for the distal tips of the dorsal and posterior articular heads, articulating with the neurocranium and opercle, respectively, which remain cartilage. The symplectic is also well-ossified, and separated from the hyomandibular only by a thin remnant of the hyosymplectic cartilage at the point of articulation with the interhyal. The quadrate and the metapterygoid are now completely ossified yet remain separated by a think remnant of the palatoquadrate cartilage. A small remnant of the pars metapterygoidea also remains between the metapterygoid and the lower arm of the hyomandibular. The autopalatine is also completely ossified but retains a small cartilaginous tip anteriorly, which articulates with the dorsal region of the maxilla. The anterior region of the

anguloarticular is now completely surrounded by the dentary. The bony ridges flanking the mandibular portion of the preopercular-mandibular sensory canal along the lateral side of the dentary are more greatly developed, but have yet to make contact across the roof of the canal. The dorsal edge of the subopercle and interopercle are now completely covered by the ventral edge of the opercle and preopercle, respectively, and a weak articulation between the two bones has now developed.

At 43.2 mm SL (Figure 2F), a stage comparable to that of the adult, the hyomandibular and symplectic are similar to the previous stage described with additional sculpturing now present on the dorsal head of the hyomandibular. The metapterygoid and quadrate are now in direct bony contact via bony sutures, which extend across the remnant strip of the palatoquadrate cartilage that separates the two bones. The ventral margin of the autopalatine has continued to expand and is now slightly curved. The endopterygoid is similar to that described for the previous stage while the posterior half of the ectopterygoid has expanded ventrally and now possesses an anteriorly directed spine-like process midway along its length. The posterior tip of the anguloarticular has extended posteriorly along the dorsal edge of the mandibular portion of the preopercular-mandibular sensory canal and is separated only by a short distance from the anterior edge of the preopercle. The bony ridges on the lateral surface of the dentary are now connected via thin struts of bone, forming three large cavernous openings in the roof of the mandibular portion of the preopercular-mandibular canal anteriorly. In addition to the small coniform teeth present earlier in earlier stages, an outer row of much larger coniform teeth has begun to form on the premaxilla. The ascending process of the premaxilla has widened with the anterior edge more rounded than in previous stages. Small bony protrusions are also present along the lateral edge of the preopercle that will later connect with the dorsal ridge and delimit the cavernous openings in the preopercular portion of the preopercular-mandibular sensory canal.

Comparison to C. nebulosus

The sequence of ossification for this region in the *C. nebulosus* is: maxilla, dentary (2.6

mm NL); opercle (3.1 mm NL); premaxilla (3.2 mm NL); symplectic (3.5 mm NL); endopterygoid, hyomandibular (3.6 mm NL); anguloarticular, ectopterygoid (3.7 mm NL); interopercle, preopercle, subopercle, quadrate (3.8 mm NL); retroarticular (4.0 mm NL); autopalatine (4.4. mm NL); metapterygoid (4.8 mm NL); and coronomecklian (6.4 mm SL).

The sequence of ossification for this region in *C. nebulosus* differed slightly from that of *S. ocellatus*. The anguloarticular develops later in *C. nebulosus*, after the hyomandibular which develops earlier just after the endopterygoid (Compared to developing after the preopercle in *S. ocellatus*). The ectopterygoid and interopercle appear at approximately the same size as the subopercle, preopercle, and quadrate in *C. nebulosus* (compared to after the retroarticular in *S.* ocellatus). Overall, the adult jaws, hyopalatine arch and opercular series of *C. nebulosus* are generally similar to that of *S. ocellatus*. The most striking difference is the enlarged fang-like tooth on the anterior edge of the premaxilla of *C. nebulosus*, which is approximately twice the length of our other premaxillary teeth. In some of the specimens, the coronomeckelian was completely absent (1), or was absent only on one side (right or left) of the lower jaw (20).

Infraorbitals

I describe four different stages in the development of the infraorbitals. The sequence of ossification for this region is: infraorbital 1 (5.9 mm SL); infraorbital 2 and infraorbital 4 (9.7 mm SL); infraorbital 3 (10.2 mm SL); and infraorbital 5 (12.1 mm SL).

In the smallest stage illustrated (8 mm SL; Figure 3A), infraorbital 1 (lacrimal) is the only element of the infraorbital series present. It is represented by a thin lamina of dermal bone, located lateral to the anterior tip of the autopalatine and ventrolateral to the lateral tip of the lamina orbitonasalis. The lateral face of infraorbital 1 is indented, giving the bone an overall cup-like appearance. Three small pits, associated with neuromast formation in the infraorbital sensory canal, are also present along the lateral face of infraorbital 1 and a small, dorsomedially directed process is also present along the

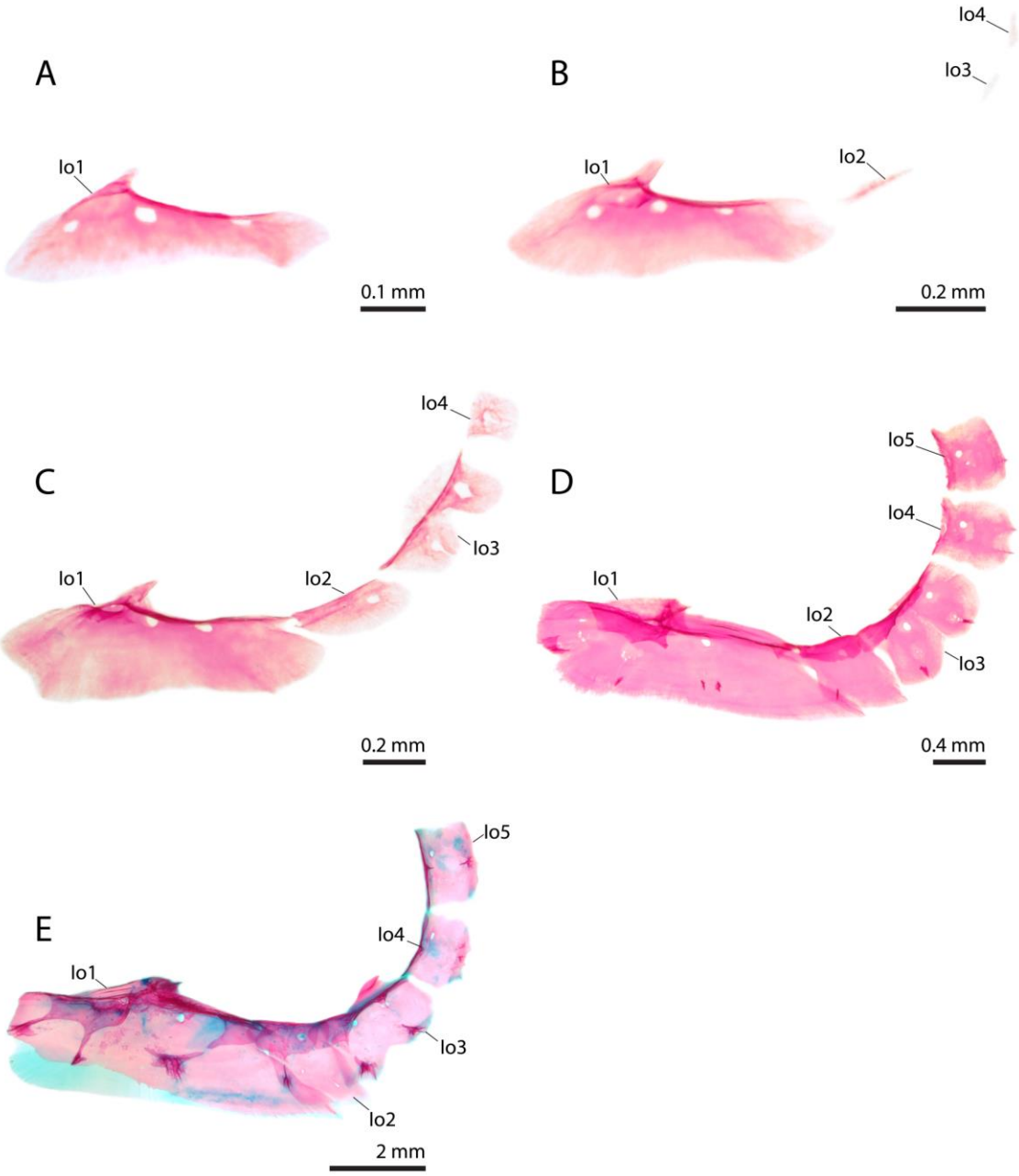

Fig. 3. Ontogeny of the infraorbitals of *S. ocellatus* (A-D, TCWC 16420.01; E, TCWC 8404.22). **A.** 8 mm SL. **B.** 9.8 mm SL. **C.** 12.6 mm SL. **D.** 23.7 mm SL. **E.** 67 mm SL. Io, Infraorbital.

anterodorsal edge of the bone.

At 9.8 mm SL (Figure 3B), infraorbital 1 has changed little in shape from the previous stage described. The dorsomedially directed extension along the anterodorsal edge of this element is now larger and has developed into a concave facet that receives the posterior tip of the lamina orbitonasalis. An additional small extension of bone is now present along the dorsal edge of infraorbital 1 that is directed ventrolaterally to cover an additional pit that has developed in association with neuromast formation in the infraorbital sensory canal on the lateral face of the bone. Infraorbitals 2, 3 and 4 are now also present and represented by thin slivers of dermal bone posterior to infraorbital 1.

At 12.6 mm SL (Figure 3C), infraorbital 1 has grown considerably but has retained a similar shape. Infraorbital 2 is now a rhomboid shaped ossification with two small pits that have developed in association with neuromast formation in the infraorbital sensory canal on the lateral face; one located close to the anterior edge and one located further posteriorly. Infraorbital 3 has developed considerably since the last stage and is now approximately the same size as infraorbital 2. The posteroventral edge of infraorbital 3 is indented, creating two rounded extensions, each with a single pit that has developed in association with neuromast formation in the infraorbital sensory canal. Infraorbital 4 is now square-shaped and exhibits a single small pit, developed in association with neuromast formation in the infraorbital sensory canal, at its center.

At 23.7 mm SL (Figure 3D), infraorbital 1 is now greatly elongated (compared to other infraorbital elements) and the ventrolaterally directed process along the dorsal edge of the bone has extended further anteriorly, partially covering the roof of the infraorbital sensory canal. Infraorbital 2 now contacts infraorbital 1 anteriorly and has expanded ventrally along its posterior half. The dorsal edges of infraorbitals 2 and 3 now extend further laterally than that of other infraorbital elements and a small suborbital sty is now present along the medial face of infraorbital 3. Infraorbital 4 is now more heavily ossified but has retained a similar shape to that of the previous stage described. Infraorbital 5 is now present as a square shaped lamina of dermal bone, similar in size

and shape to infraorbital 4, and contains a single pit, developed in association with neruomast formation in the infraorbital sensory canal, at the center of the bone. All infraorbitals now possess small bony protrusions, representing the first signs of the bony struts that will later roof the infraorbital sensory canal, along their lateral edges.

At 67 mm SL (Figure 3E), a stage comparable to that of the adult, extensive sculpturing is now present on the bony protrusions present on infraorbitals 1-3. The two anteriormost cavernous openings in the infraorbital sensory canal are now delimited via thin bony struts, which connect the two anteriormost bony protrusions on the lateral face of infraobrital 1 with the ventrolaterally directed process along the dorsal edge of the bone. Similar bony struts have developed on more posterior bony protrusions on infraorbital 1 and also on those of infraorbital 2 and 3 but they have yet to make contact with the ventrolateral rim of bone present the dorsal edge of these elements. The suborbital sty of infraorbital 3 is now much larger and more heavily ossified and extends further medially to rim the posteroventral margin of the orbit.

Comparison to C. nebulosus

The sequence of ossification for this region in *C. nebulosus* is: infraorbital 1 (6.1 mm SL); infraorbital 2 (9.5 mm SL); infraorbital 3 (10.2 mm SL); infraorbital 4 (12.4 mm SL); and infraorbital 5 (13.7 mm SL).

The sequence of ossification for this region in *C. nebulosus* differed from that of *S. ocellatus*. In *C. nebulosus*, infraorbital 3 develops before infraorbital 4. Additionally, Infraorbitals 4 and 5 develop at larger sizes in the spotted seatrout than in the red drum. The adult infraorbital series of *C. nebulosus* is generally similar to that of *S. ocellatus*. The most striking difference is the shape of infraorbital 3, the ventral edge of which is entire in *C. nebulosus* and indented in *S. ocellatus*.

Gill Arches

I describe four different stages in the development of the gill arches. The sequence of ossification for this region is: pharyngobranchial 3 toothplate (3.1 mm NL);

ceratobranchial 1 and ceratobranchial 2 (3.2 mm NL); ceratobranchial 3 (3.5 mm NL); ceratobranchial 4 (3.6 mm NL); ceratobranchial 5 (3.8 mm SL); epibranchial 3, epibranchial 4, pharyngobranchial 2 toothplate and pharyngobranchial 4 toothplate (4.5 mm NL); epibranchial 1 and epibranchial 2 (4.6 mm NL); gill rakers and hypobranchial 1 (4.9 mm SL); pharyngobranchial 3 (5 mm SL); basibranchial 3 and hypobranchial 2 (5.3 mm SL); hypobranchial 3 (6 mm SL); basibranchial 2 (6.7 mm SL); pharyngobranchial 2 (7.4 mm SL); basihyal (8.9 mm SL); pharyngobranchial 1 (9.2 mm SL); and basibranchial 1 (9.7 mm SL).

In the smallest stage illustrated (4.5 mm NL; Figure 4A), all cartilaginous elements of the gill arch endoskeleton, excluding the basihyal cartilage, are present. In the lower gill arch endoskeleton, the copula communis is represented by a rod shaped cartilage located anteriorly along the ventral midline of the gill arches. Three pairs of hypobranchial cartilages, decreasing in size from anterior to posterior, flank the copula communis laterally. The two anteriormost hypobranchial cartilages (Hb1-2 cartilages) are short, roughly rod-shaped elements whereas the posteriormost hypobranchial cartilage (Hb3 cartilage) is a small, round element, with a short anteroventral extension. The posterior copula is represented by a small round cartilage, situated along the ventral midline of the gill arches posterior to the posteromedial tip of hypobranchial 3 cartilage and anterior to the anteromedial tip of the ceratobranchial 4 cartilage. The five ceratobranchial cartilages are long, roughly rod-shaped elements that decrease in length from anterior to posterior. The anteromedial tips of ceratobranchials 1-3 cartilages articulate with the posterolateral heads of hypobranchials 1-3 cartilages, whereas the anteromedial tip of ceratobranchial 4 cartilage articulates with the posterolateral edge of the posterior copula. The earliest signs of ceratobranchials 1-5 are present as perichondrally ossified bone around the mid-length of their respective cartilages. Minute conical teeth are present in the epithelium dorsal to the perichondral ossification of ceratobranchial 5 but are not yet in direct contact with this element. In the upper gill arch endoskeleton, four epibranchial cartilages, represented by four, roughly rod-shaped elements that decrease in length from anterior to posterior, and four pharyngobranchial cartilages are present.

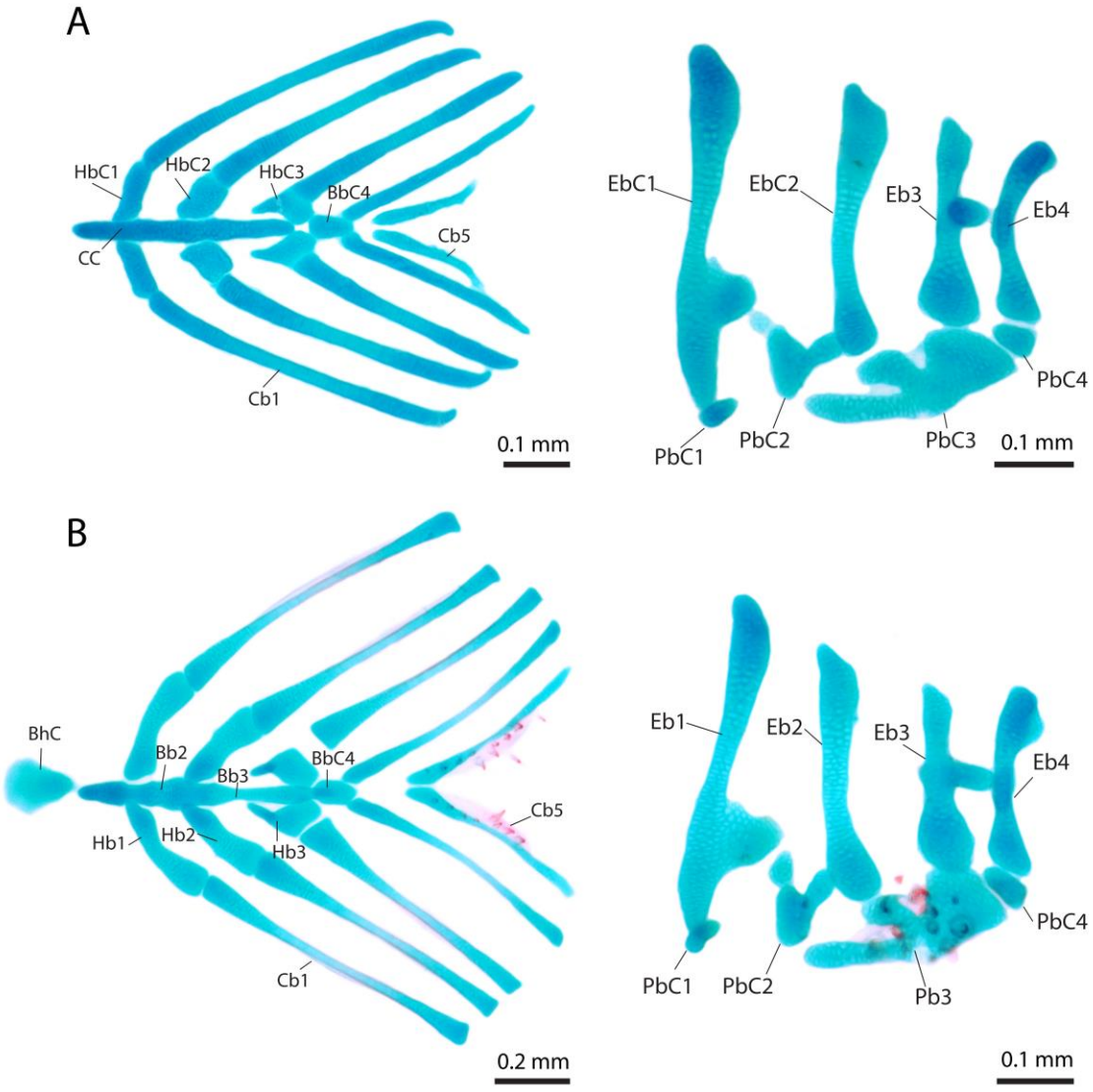

Fig. 4. Ontogeny of the gill arches of *S. ocellatus* (A-C, TCWC 16420.01; D, TCWC 12308.24). **A.** 4.5 mm NL. **B.** 7 mm SL. **C.** 11.7 mm SL. **D.** 24.1 mm SL. Bb, Basibranchial; BbC, Basibranchial Cartilage; Bh, Basihyal; BhC, Basihyal Cartilage; Cb, Ceratobranchial; CC, Copular Communalis; Eb, Epibranchial; EbC, Epibranchial Cartilage; Hb, Hypobranchial; HbC, Hypobranchial Cartilage; Pb, Pharyngobranchial; PbC, Pharyngobranchial Cartilage.

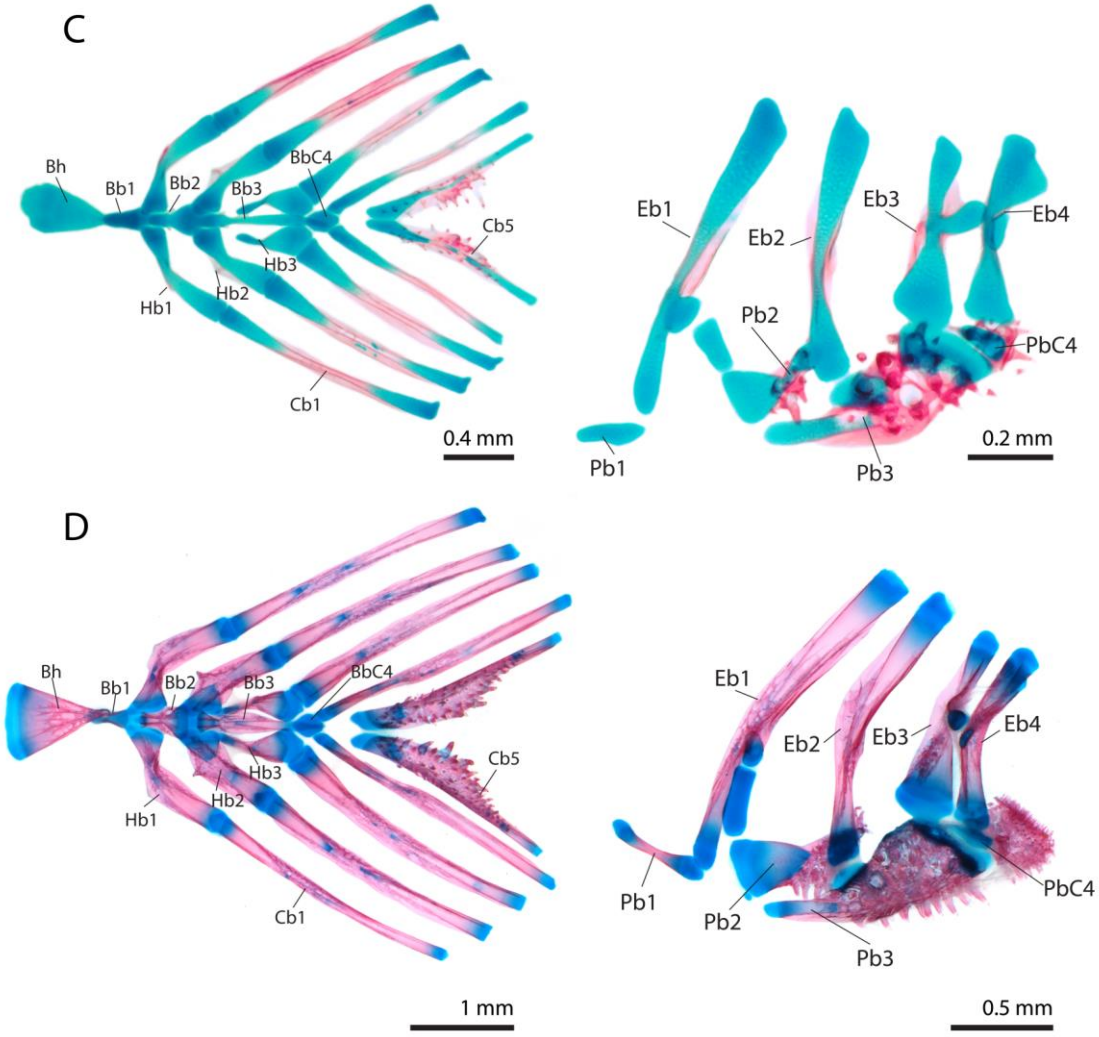

Fig. 4. Continued

Epibranchial 1 cartilage articulates medially with the small nodular pharyngobranchial 1 cartilage. A large cartilaginous uncinate process is present along the posterior edge of epibranchial 1 cartilage, close to the medial tip. A small nodule of cartilage, representing the interarcular cartilage, is located between the tip of this uncinate process and the anterolateral tip of pharyngobranchial 2 cartilage. Epibranchial 2 cartilage articulates

anteromedially with the posterior tip of pharyngobranchial 2 cartilage and medially with lateral arm of pharyngobranchial 3 cartilage. Epibranchial 3 cartilage articulates medially with the enlarged posterolateral margin of pharyngobranchial 3 cartilage. A large cartilaginous uncinate process is present along the posterior edge of epibranchial 3 cartilage that is extended posteriorly, towards the anterior edge of epibranchial 4 cartilage. Epibranchial 4 cartilage, the smallest of the epibranchial cartilages, articulates medially with the small pharyngobranchial 4 cartilage. The earliest signs of epibranchials 3-4 are represented by perichondrally ossified bone around the midlength of epibranchial 3-4 cartilages. Dermal toothplates are situated ventral to pharyngobranchial 2-4 cartilages. Pharyngobranchial 3 toothplate is the largest of the three toothplates and exhibits several small conical teeth over its ventral surface. Pharyngobranchial 2 and 4 toothplates are much smaller than pharyngobranchial 3 toothplate and exhibit one and two small conical teeth, respectively, at this stage.

At 7 mm SL (Figure 4B), the copula communis exhibits slight lateral bulges adjacent to the anteromedial tips of hypobranchials 1 and 2 and now terminates ventral to the anterior edge of the posterior copula. The basihyal cartilage is now present and situated anterior to the copula communis, from which it is separated by a short gap. Basibranchials 2-3 are now present as perichondrally ossified bone around the copula communis and basibranchial 3 has also started to ossify endochondrally within the copula communis. Hypobranchials 1-3 are now present as perichondrally ossified bone around their respective cartilages. Ceratobranchials 1-5 have grown in length and have begun to ossify endochondrally. Thin extensions of membrane bone also are now present along both the anterior and posterior margins of ceratobranchials 1-5 and a single row of small gill rakers is closely associated with the membrane bone extensions along both the anterior and posterior margins of ceratobranchials 1-4. Numerous small conical teeth, arranged in a single row, are now associated with ceratobranchial 5. Epibranchials 1-2 are now present as perichondrally ossified bone around the midlength of their respective cartilages. The uncinate processes on the posterior edge of epibranchial 1 and epibranchial 3 cartilages have grown considerably and the uncinate process on

epibranchial 3 cartilage is now in direct contact with the anterior edge of epibranchial 4 cartilage. Pharyngobranchial 3 has begun to ossify perichondrally around the anterior arms of pharyngobranchial 3 cartilage. Pharyngobranchial 3 toothplate has extended beyond the margin of pharyngobranchial 3 cartilage and multiple teeth are now associated with all three pharyngobranchial toothplates.

At 11.7 mm SL (Figure 4C), all three basibranchial elements are now ossified perichondrally around the copula communis but remain separated by wide expanses of cartilage. Basibranchial 3 now exhibits small lateral extensions of membrane bone but, overall, retains the original rod-like shape of the cupula. Basibranchial 2 is also now ossified endochondrally and possesses two small wing-like extensions of membrane bone anteriorly. Basibranchial 1 is represented by a small cap of perichondrally ossified bone around the anteriormost tip of the copula. The basihyal is now ossified perichondrally around the basihyal cartilage, which has also begun to ossify endochondrally posteriorly, close to the point of articulation basibranchial 1. All three hypobranchials are now ossified endochondrally at their mid-length and exhibit flanges of membrane bone along both anterior and posterior margins. Membrane bone now extends along much of the anterior and posterior margins of ceratobranchials 1-5. The flange of membrane bone along the posterior edge of ceratobranchial 5 is more extensively developed than that of other ceratobranchial elements and now supports multiple rows of small conical teeth, with the majority of teeth concentrated around the mid-length of the membrane bone flange along the posterior edge of the bone. All four epibranchials have begun to ossify endochondrally and now possess flanges of membrane bone along their mid-length. Much of pharyngobranchial 3 is now ossified endochondrally, with cartilage remaining only along the broad posterior margin and the anteriormost tips of the two anterior arms. Pharyngobranchials 1 and 2 are now ossified perichondrally around their respective cartilages and pharyngobranchial 2 has begun to ossify endochondrally within the center of pharyngobranchial 2 cartilage. Multiple rows of small conical teeth now cover most of the available space on the ventral surface of all three of the pharyngobranchial toothplates.

At 24.1 mm SL (Figure 4D), a stage comparable to that of the adult, all elements of the lower gill arches are now heavily ossified and exhibit extensive surface sculpturing but retain cartilaginous tips. The posterior copula persists as basibranchial 4 cartilage. The membrane bone flanges along the lateral edges of basibranchial 3 and basibranchial 2 now extend almost the full length of the elements. Hypobranchial 2 now exhibits an anteriorly directed spine-like process located at its midlength. Ceratobranchial 5 is now completely ossified with the membrane bone now extending further medially with the teeth along the medial edge now significantly larger than the others. The epibranchials are now completely ossified and possess sculpturing at their mid-region but retain cartilaginous tips where they articulate with other elements of the gill arches. A toothpatch of small conical teeth is now present on the ventral surface of epibranchial 3. The interarcular cartilage has grown considerably and is now rod-like in appearance. Pharyngobranchial 4 cartilage remains without ossification. Pharyngobranchials 1 and 2 are now fully ossified endochondrally but retain cartilaginous tips. Pharyngobrancial 4 toothplate has grown considerably and now extends posteriodorsally around pharyngobranchial 4 cartilage and is in direct contact with the medial tip of epibranchial 4. Pharyngobranchial 2 and 3 toothplates are now fused with Pharyngobranchials 2 and 3, respectively.

Comparison to C. nebulosus

The sequence of ossification for this region in the spotted seatrout is: ceratobranchial 1, ceratobranchial 2 (3.0 mm NL); ceratobranchial 3, pharyngobranchial 3 toothplate (3.3. mm NL); ceratobranchial 4 (3.6 mm NL); ceratobranchial 5 (3.8 mm NL); epibranchial 1, epibranchial 2, epibranchial 3, epibranchial 4 (3.8 mm NL); hypobranchial 1 (4.0 mm NL); pharyngobranchial 2 toothplate, pharyngobranchial 3, pharyngobranchial 4 toothplate (4.4 mm NL); gill rakers (4.7 mm NL); hypobranchial 2 (4.7 mm NL); basibranchial 3 (5.3 mm SL); basibranchial 2, hypobranchial 3 (5.5 mm SL); pharyngobranchial 2 (6.6. mm SL); basibranchial 1 (6.8 mm SL); basihyal and pharyngobranchial 1 (6.9 mm SL).

The sequence of ossification for this region in *C. nebulosus* differed slightly from that of *S. ocellatus*. Pharyngobranchial 3 toothplate develops later in *C. nebulosus,* after ceratobranchial 2 has developed and before ceratobranchial 3. All four epibranchials appear at approximately the same time (compared to epibranchials 3 and 4 developing before epibranchials 1 and 2 in *S. ocellatus*) and pharyngobranchial 3 appears at the same time as pharyngobranchial 2 and pharyngobranchial 4 toothplate. Hypobranchial 1 develops much earlier in *C. nebulosus,* after the epibranchials have developed (compared to later after the gillrakers in *S. ocellatus*). Hypobranchial 2 develops before basibranchial 3, whereas hypobranchial 3 and basibranchial 2 appear at the same time (compared to hypobranchial 3 developing earlier than basibranchial 2 in *S. ocellatus*). Finally, basibranchial 1 develops before the basihyal in *C. nebulosus* (compared to after the basihyal in *S. ocellatus*). The gill arches of *C. nebulosus* and *S. ocellatus* are generally similar and no major differences in adult morphology for this region were identified.

Hyoid Bar

I describe four different stages in the development of the hyoid bar. The sequence of ossification for this region is: anterior ceratohyal (3.1 mm NL); urohyal (4 mm NL); branchiostegal rays, interhyal, posterior ceratohyal (4.8 mm SL); ventral hypohyal (5 mm SL); and dorsal hypohyal (7.3 mm SL).

In the smallest stage illustrated (3.8 mm SL; Figure 5A), the ceratohyal cartilage is present as a rod of cartilage that is considerably deeper posteriorly than anteriorly. Anteriorly, the ceratohyal cartilage contacts the hypohyal cartilage, which is represented by a small, roughly square-shaped cartilage with a shallow groove along the posterodorsal edge that accommodates the hyoid artery. Posteriorly, the ceratohyal cartilage is in contact with the small, rod-like interhyal cartilage. A small triangular projection is also present along the dorsal surface of the posterior part of the ceratohyal cartilage, slightly anterior to the point of contact with the interhyal cartilage. The anterior ceratohyal is present as a poorly developed perichondral ossification around

Fig. 5. Ontogeny of the hyoid bar of *S. ocellatus* (TCWC 16420.01). **A.** 3.8 mm NL. **B.** 5.3 mm SL. **C.** 11.7 mm SL. **D.** 25.3 mm SL. Ach, Anterior Ceratohyal; Br, Branchiostegal Ray; DHh, Dorsal Hypohyal; HhC, Hypohyal Cartilage; Ih, Interhyal; IhC, Interhyal Cartilage; PCh, Posterior Ceratohyal; Uh, Urohyal; VHh, Ventral Hypohyal.

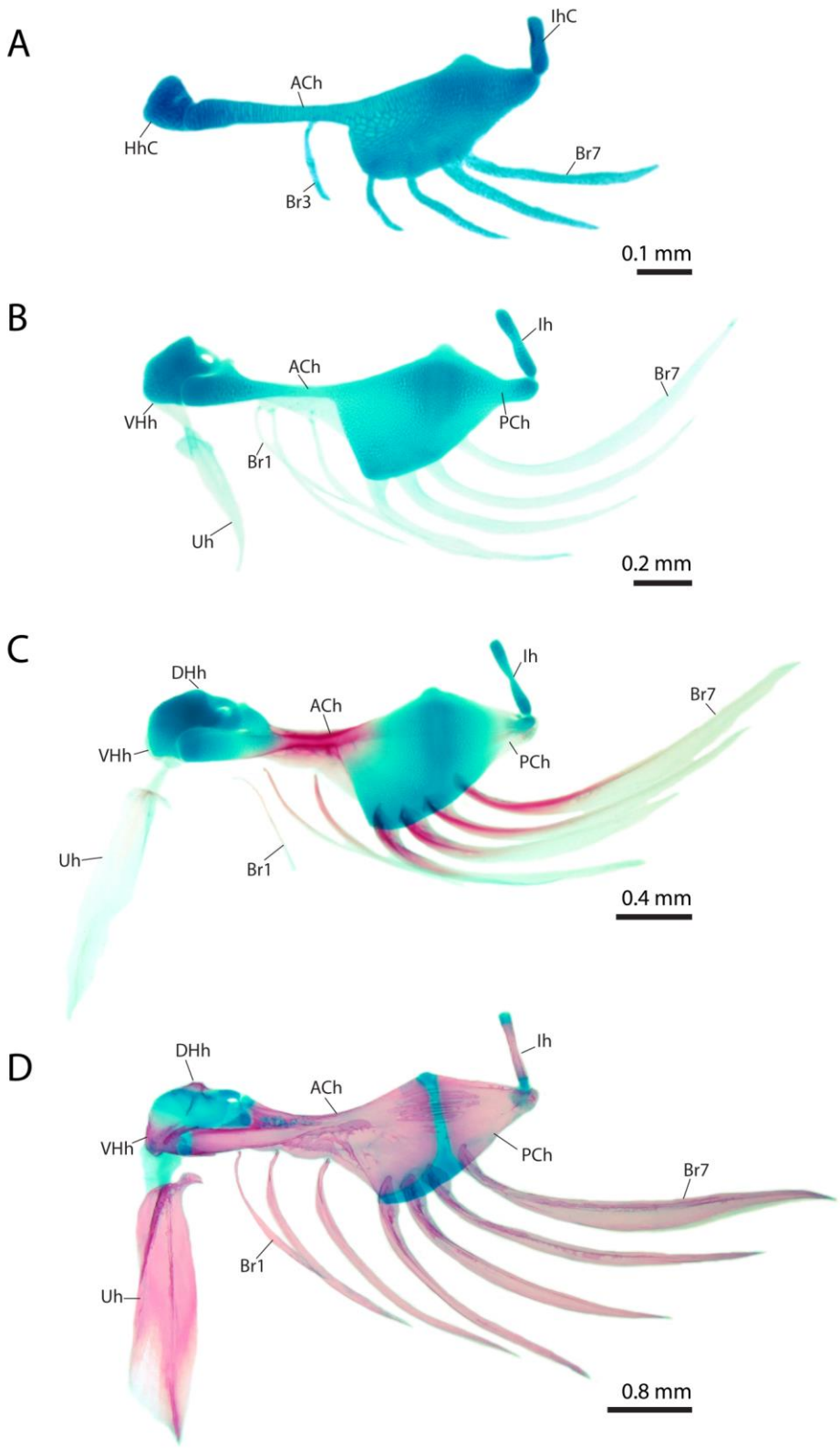
A
IhC
ACh
HhC
Br7
Br3
0.1 mm
B
Ih
ACh
Br7
VHh
PCh
Br1
Uh
0.2 mm
C
DHh
Ih
ACh
Br7
VHh
PCh
Uh
Br1
0.4 mm
D
DHh
Ih
ACh
VHh
PCh
Br7
Br1
Uh
0.8 mm

much of the narrow anterior portion of the ceratohyal cartilage. Four branchiostegal rays (corresponding to branchiostegal rays 4-7 of the adult) are present as thin slivers of dermal bone articulating along the lateral face of the deeper posterior portion of the ceratohyal cartilage. A fifth branchiostegal ray (corresponding to branchiostegal ray 3 of the adult) is located ventral to the anterior ceratohyal, articulating with the medial face of the ceratohyal cartilage.

At 5.3 mm SL (Figure 5B), the perichondral ossification of the anterior ceratohyal now covers a much larger portion of the ceratohyal cartilage. Thin slivers of membrane bone are also now present along both the dorsal and ventral surface of the anterior ceratohyal. The posterior ceratohyal is now present as thin perichondrally ossified bone around the posterior portion of the ceratohyal cartilage. The hypohyal cartilage is now much larger and extends posteriorly to dorsally overlap the anterodorsal edge of the ceratohyal cartilage, which now exhibits a small dorsal extension that abuts the posterodorsalmost tip of the hypohyal cartilage. Cartilage cells have now enclosed the groove present along the posterodorsal edge of the hypohyal cartilage, forming a foramen for the passage of the hyoid artery. The poorly developed ventral hypohyal is now present as a thin perichondral ossification around the anteroventral margin of the hypohyal cartilage. The interhyal is now present as a perichondral ossification around the midlength of the interhyal cartilage. All seven branchiostegal rays are now present, with the four posteriormost rays (4-7) much larger than the three anterior rays (1-3), which are each represented by tiny slivers of dermal bone. The urohyal is now present as a triangular shaped, anteriorly bifurcated ossification present within the ligament of the sternohyoideus muscle.

At 11.7 mm SL (Figure 5C), the anterior ceratohyal is now ossified endochondrally at its midlength and the membrane bone flanges along its dorsal and ventral surface are weakly sculptured. The dorsal extension along the anterodorsal edge of the ceratohyal cartilage is now considerably larger and now abutts against the entire posterodorsal margin of the hypohal cartilage. The posterior ceratohyal is now also ossified

endochondrally posteriorly in the ceratohyal cartilage and a thin flange of membrane bone is now present along the posteroventral margin of the bone. The dorsal hypohyal is now present as a thin perichondral ossification around the dorsalmost point of the hypohyal cartilage. The interhyal is also now ossified endochondrally at its mid-length. Sculpturing is now present across the lateral face of articulatory heads of the four posteriormost branchiostegal rays. The urohyal has grown considerably and also now possesses a short dorsal extension anteriorly.

At 25.3 mm SL (Figure 5D), a stage comparable to that of the adult, the anterior ceratohyal has now almost completely replaced the anterior portion of the ceratohyal cartilage, which is now represented only by a small remnant of cartilage along the anterior edge of the anterior ceratohyal and as a strip of cartilage that runs between the anterior and posterior ceratohyals and extends anteroventrally to rim the posteroventral margin of the anterior ceratohyal. Similarly, the posterior ceratohyal has now completely replaced the posterior portion of the ceratohyal cartilage. Small sutures are now present between the posterior edge of the anterior ceratohyal and the anterior edge of the posterior ceratohyal, lateral to the remnant of the ceratohyal cartilage that separate the two bones. The ventral hypohyal has now almost completely replaced the entire anteroventral portion of the hypohyal cartilage and the perichondral ossification of the dorsal hypohyal now caps the entire dorsal surface of the hypohyal cartilage. The dorsal hypohyal also now exhibits endochondrally ossified components dorsally. The interhyal has now replaced much of the interhyal cartilage, which is now represented only by small caps of cartilage at the points of articulation between the interhyal and the hyomandibular, dorsally, and the posterior ceratohyal, ventrally. The narrow articulatory heads of the three anteriormost branchiostegal rays now articulate directly with grooves along the ventromedial face of the anterior ceratohyal. Sculpturing is also now present along the entire lateral face of the four anteriormost branchiostegal rays. The urohyal now exhibits a large dorsal crest along the midline and a well-developed ridge is also now present along the lateral face of the bone. The anterodorsal process of the urohyal is now greatly pronounced and sculpturing is now present anteriorly.

Comparison to C. nebulosus

The sequence of ossification for this region in *C. nebulosus* is: anterior ceratohyal (2.8 mm NL); urohyal (3.8 mm NL); interhyal (4.4. mm NL); branchiostegal rays, posterior ceratohyal (4.7 mm NL); ventral hypohyal (4.8 mm NL); and dorsal hypohyal (6.8 mm SL).

The sequence of ossification for this region in *C. nebulosus* is very similar to that of *S. ocellatus*, differing only in one aspect. In *C. nebulosus*, the interhyal develops before branchiostegal ray 1 has formed whereas in *S. ocellatus* the interhyal does not appear until after branchiostegal ray 1 is present. The hyoid bar of *C. nebulosus* and *S. ocellatus* are similar and no major differences in adult morphology for this region were identified.

Vertebral Column

I describe four different stages in the development of the vertebral column excluding preural centra 2 and 3. The sequence of ossification for this region is: neural arch 1, neural arch 2, centrum 1, centrum 2, centrum 3, centrum 4 and centrum 5 (4.4 mm SL); neural arch 3, neural arch 4, neural arch 5, neural spine 1, neural spine 2 and neural spine 3 (4.8 mm NL); neural spine 4 and neural spine 5 (4.9 mm NL); remaining centra (5.2 mm SL); hemal arches (5.6 mm SL); remaining neural arches (5.8 mm SL); hemal spines and remaining neural spines (6 mm SL); ribs (7.8 mm SL); supraneural 3 (8.3 mm SL); supraneural 2 and epicentrals (8.9 mm SL); and supraneural 1 (10 mm SL).

In the smallest stage illustrated (4 mm NL; Figure 6A) the only two elements present are the basidorsals of centrum 1 and 2. Both elements are present as a pair of rod-like cartilages that flank the anteriormost part of the notochord dorsolaterally.

At 4.5 mm NL (Figure 6B) the vertebral column has developed extensively beyond that described for the previous stage. The first 14 centra are now present as chordocentra. Centra 1-4 begin ossifying at the base of the neural arch cartilages and proceed in a ventral direction until a complete ring of ossification has formed around the notochord. Centra 1-3 ossify at a much slower rate compared to centrum 4, and appear as saddles of

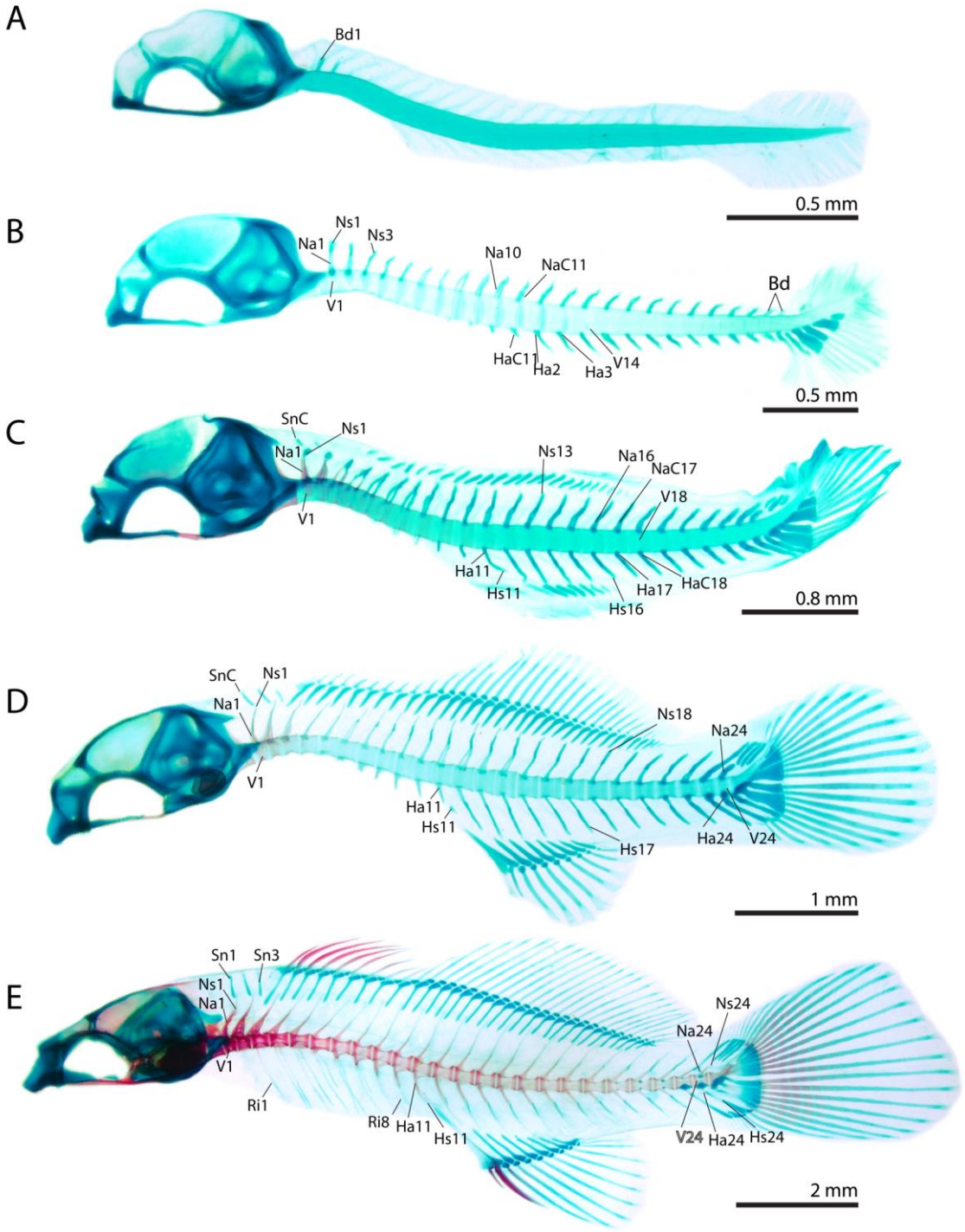

Fig. 6. Ontogeny of the vertebral column of *S. ocellatus* (TCWC 16420.01). **A.** 4 mm NL. **B.** 4.5 mm NL. **C.** 5.1 mm SL. **D.** 5.9 mm SL. **E.** 12.6 mm SL. Bd, Basidorsal; Ha, Hemal Arch; HaC, Hemal Arch Cartilage; Hs, Hemal Spine; HsC, Hemal Spine Cartilage; Na, Neural Arch; NaC, Neural Arch Cartilage; Ns, Neural Spine; NsC, Neural Spine Cartilage; Sn, Supraneural; SnC, Supraneural Cartilage; V, Vertebral Centrum.

ossification along the dorsal surface of the notochord anterior to the complete ring of ossification represented by centrum 4. The remaining centra (excluding PU3 and PU2) begin ossifying ventrolaterally and proceed in a dorsal direction until a complete ring of ossification has formed around the notochord. The first twenty two basidorsals and all of the basiventrals have fused along the midline to form neural arch and hemal arch cartilages respectively. Neural arches 1-10 and hemal arches 2 and 3 are now ossified perichondrally at the midlength of their respective cartilages. The first 22 neural spine cartilages and all 14 hemal spine cartilages are now formed at the distal tips of their respective neural and hemal arch cartilages with neural spines 1-3 now perichondrally ossified distally. Small cartilaginous parapophyses are now associated with the ventrolateral margin of centra 8-10 and appear to develop in an anterior direction.

At 5.1 mm SL (Figure 6C), centra 1-18 are now present. Neural arches 1-16 are now ossified perichondrally with the first six now ossified endochondrally as well. Ten additional neural spines are now present bringing the total to thirteen. The anteriormost two neural spines are now almost fully ossified with only a small remnant of the neural spine cartilage remaining in contact with the neural arches. Hemal arches 1-7 are now ossified around the midlength of their respective hemal arch cartilages. In addition, the first six hemal spines are now present as perichondral ossifications around the midlength of the cartilage. The parapophyses of centra 8-10 have grown considerably since the last stage with 5 and 6 now meeting their antimere across the midline and ossifying perichondrally. Two additional cartilaginous parapophyses are now associtated with centra 6 and 7. Two small cartilages representing supraneural 1 and 2 cartilages are now present anterodorsal to the neural spines of the first two centra.

At 5.9 mm SL (Figure 6D), all centra are now present but have yet to attain the hourglass shape typical of teleosts. All neural and hemal arches are now ossified with small remnants of the neural and hemal arch cartilages restricted to the base of the arches. Additionally, the first three neural arches have begun to widen proximally. Neural spines 1-18 are now perichondrally ossified and have begun to endochondrally ossify distally.

Hemal spines 1-7 have also ossified in the same manner as the neural spines. All six parapophyses are now present with the anteriormost positioned slightly more dorsally on the associated centrum than proceeding parapophyses. Supraneural cartilage 3 is now present posterior to supraneural cartilage 2 and anterodorsal to neural spines 3.

In the final stage illustrated (12.6 mm SL; Figure 6E), a stage comparable to that of the adult, the centra have now attained the hourglass shape of typical teleosts. Centra 1-20 now exhibit ventrolateral flanges of membrane bone. At this stage the neural and hemal arches are completely ossified with the exception of the posterior most elements, which retain a remnant of the neural and hemal arch cartilages near the base of the elements. Neural arches 1-4 have continued to widen and now possess sculpturing along the lateral surface. All neural and hemal spines are ossified with some cartilage still remaining at the base on the elements associated with centra 12-22. The first hemal spine now possesses a large flange of membrane bone that extends posteroventrally, terminating just dorsal to the proximal tip of the proximal radial of the first anal fin pterygiophore. Eight pairs of ribs are now present, with the first two articulating directly with the lateral face of centra 3 and 4, and the remaining six articulating with parpophyses associated with centra 5-10. Seven pairs of poorly ossified epicentrals are also present at this stage. The first two pairs articulate directly with the base of neural arches 1 and 2, and the remaining five connect with ribs 3-7 via a short ligament. All centra now possess paired prezygapophyses and postzygapophyses near the base of the neural and hemal arches. All three supraneurals have begun to ossify perichondrally around the midlength of the supraneural cartilages. Supraneurals 2-3 also exhibit poorly developed flanges of membrane bone along the anterior margin.

Comparison to C. nebulosus

The sequence of ossification for this region in *C. nebulosus* is: neural arch 1 (3.8 mm NL); neural arch 2, neural arch 3, centrum 1, centrum 2, centrum 3, centrum 4, centrum 5, neural arch 4 (4.4 mm NL); neural arch 5, neural spine 1, neural spine 2, neural spine 3, neural spine 4, neural spine 5 (4.7 mm NL); remaining centra, excluding PU2 and

PU3, remaining hemal arches, remaining neural arches, hemal spines, excluding those associated with PU2 and PU3 (5.9 mm SL); remaining neural spines (6.1 mm SL); ribs, epicentrals (7.9 mm SL); supraneural 2 (8.9 mm SL); supraneural 3 (9.5 mm SL); and supraneural 1 (20.8 mm SL).

The sequence of ossification for this region in *C. nebulosus* differed slightly from that of *S. ocellatus*. Neural arch 3 develops at the same time as the first two neural arches and centra 1-5 in *C. nebulosus* (compared to after these elements in *S. ocellatus*). The epicentrals develop after the ribs (compared to appearing at the same time as supraneural 2 in *S. ocellatus*) and supraneural 3 develops after supraneural 2 (compared to earlier than supraneural 2 in *S. ocellatus*). Other than differences in the number of vertebrae, ribs and epicentrals, the adult vertebral column of *C. nebulosus* is generally similar to that of *S. ocellatus*. An obvious difference that exists between the two species is the variation in the number of supraneurals present in *C. nebulosus*. Three separate conditions are present in the specimens examined, including: supraneural 1 present (Fig. 7G); supraneural 1 absent but supraneural 1 cartilage present (Fig. 7F); and both supraneural 1 and supraneural 1 cartilage absent (Fig. 7E). Three supraneurals were invariably present in the specimens of *S. ocellatus* examined.

Dorsal Fin

I describe four different stages in the development of the dorsal fin. The sequence of ossification for this region is: soft rays, spiny rays (6.0 mm SL); proximal radials (7.8 mm SL); and distal radials (12.4 mm SL).

In the smallest stage illustrated (5.4 mm SL, Figure 7A), approximately 30 small rod-shaped proximal radial cartilages and 15 dorsal-fin rays are present. The dorsal-fin rays are poorly ossified and unsegmented, and retain actinotrichia at their tips. The small anteriormost fin ray present at this stage (which is approximately ¼ the length of the longest rays present towards the center of the series) is serially associated with the tenth proximal radial in the series, suggesting (based on comparison with later stages) that this

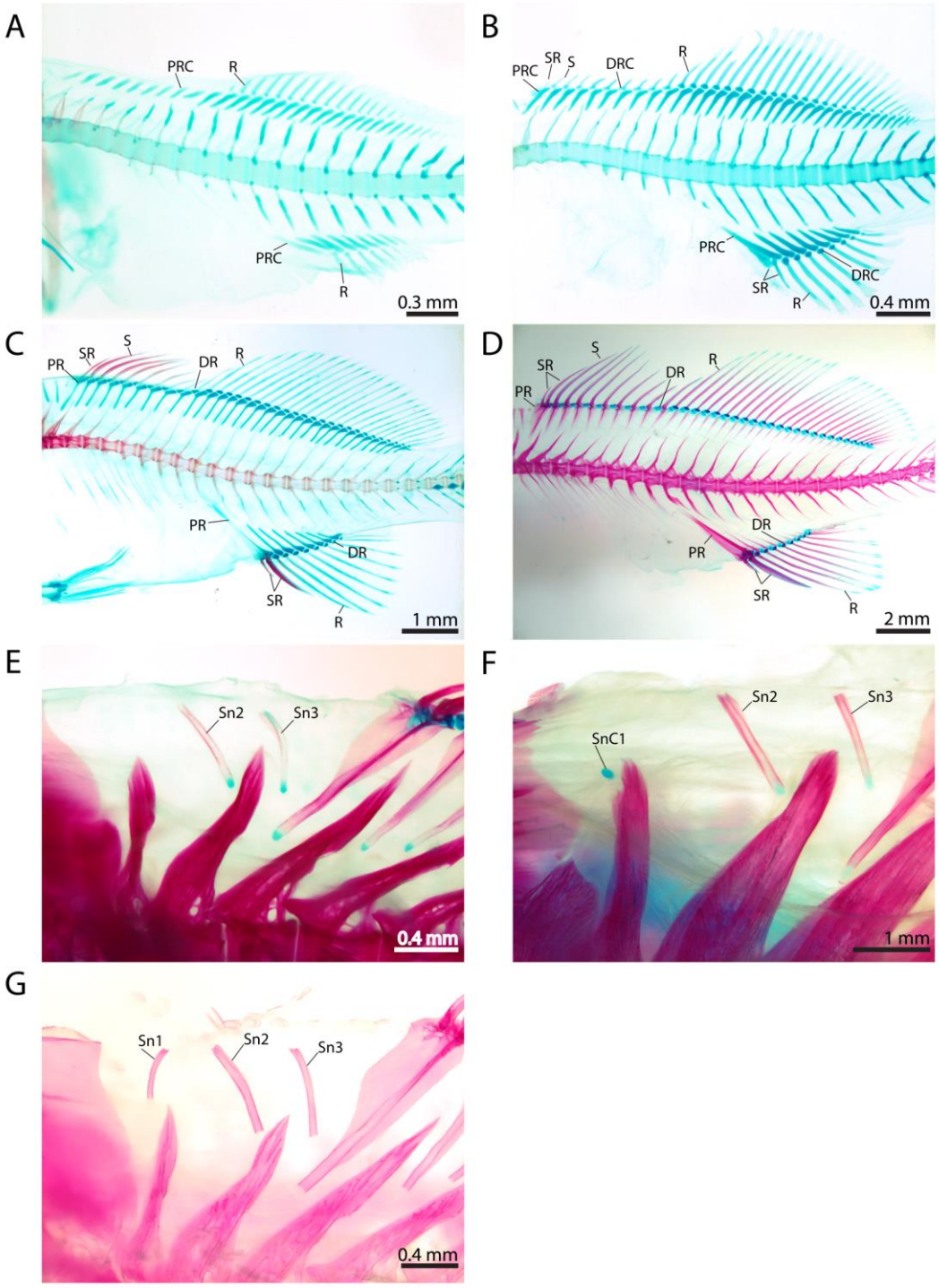

Fig. 7. Ontogeny of the dorsal and anal fins of *S. ocellatus* (A-D, TCWC 16420.01) and supraneurals of *C. nebulosus* (E-G). **A.** 5.4 mm SL. **B.** 5.9 mm SL. **C.** 12.6 mm SL. **D.** 24.1 mm SL. Variations of supraneural 1 observed in *Cynoscion nebulosus*. **E.** Supraneural 1 absent; TCWC 16422.01, 21.4 mm SL. **F.** Supraneural 1 cartilage present; TCWC 11202.23, 69.0 mm SL. **G.** Supraneural 1 fully ossified; TCWC 16423.01, 25.8 mm SL. DR, Distal Radial; DRC, Distal Radial Cartilage; PR, Proximal Radial; PRC, Proximal Radial Cartilage; R, Soft Ray; S, Spiny Ray; SR, Supranumerary Spine.

ray represents the anteriormost ray of the soft portion of the dorsal fin. Spinous dorsal-fin rays and distal radial cartilages have yet to form.

At 5.9 mm SL (Figure 7B), 34-35 proximal radial cartilages are now present, together with 29-30 distal radial cartilages, 10 spinous dorsal-fin rays and 23-24 soft dorsal-fin rays. Proximal radial cartilages towards the middle of the series are also the largest of the series and there is a pronounced bidirectional decrease in the size of these elements, from the center towards the anterior and posterior, with the exception of the first proximal radial cartilage, which is slightly larger than the second due to the presence of a thin plate of cartilage along its anterodorsal edge. All but the five posteriormost proximal radial cartilages are now associated with a small distal radial cartilage. Distal radial cartilages associated with the spinous dorsal-fin rays are distinctly triangular in shape compared to the spherical distal radial cartilages associated with the rays in the soft posterior portion of the dorsal fin. Ten spinous dorsal-fin rays are now present, with nine in serial association with the first nine pterygiophore elements and one (the first) in supernumerary association with the thin plate of cartilage along the anterior edge of the first proximal radial. Only the last spinous ray (in serial association with the ninth pterygiophore) is singular and the nine anteriormost spinous rays have yet to fuse with their antimere across the midline. The majority of the soft dorsal-fin rays are now present, with only a few of the posteriomost rays that are present in later stages absent at this stage in development. The earliest soft rays to develop (though located towards the middle of the soft portion of the dorsal fin) have begun to segment proximally.

At 12.6 mm SL (Figure 7C), all of the proximal radials are now ossified perichondrally around the proximal radial cartilages. The first five proximal radials are also ossified endochondrally at their mid length and exhibit well-developed lateral keels of membrane bone. The thin plate of cartilage present on the anterior edge of the first proximal radial has increased in size and now exhibits a slightly curved anterior projection. The posteriormost proximal radial cartilage now exhibits a short posterior extension of cartilage (dorsal-fin stay sensu Weitzman, 1962) that extends ventral to, and surpasses,

the posteriormost distal radial cartilage. All distal radial cartilages are now embraced by a single spinous or soft dorsal-fin ray, with the exception of the posteriormost, which is associated with the bases of the last two rays. The three anteriormost distal radials of the spiny dorsal fin are now ossified perichondrally around their respective distal radial cartilages. All spines present are now fused but retain a groove along the posterior edge. The spinous rays in serial association with the second to fourth distal radial elements are the longest, with a marked decrease in spinous ray length both anteriorly and posteriorly, with the exception of the ultimate spine, which is longer than the penultimate.

At 24.1 mm SL (Figure 7D), a stage comparable to that of the adult, all pterygiophore elements are now comprised of a proximal radial and a distal radial or distal radial cartilage. All proximal radials are now well ossified, except for the distalmost tips, which remain cartilaginous. Well-developed lamina of membrane bone are also now present along the entire anterior and posterior margins of each proximal radial. The anteriormost, triangular-shaped distal radials associated with the spinous dorsal-fin rays now exhibit short lateral keels, which articulate with the medial face of the bases of the spinous rays. The spherical distal radials associated with the rays of the soft portion of the dorsal fin are restricted to the lateral margins of their respective distal radial cartilages, adjacent to the medial face of the bases of the rays (i.e., each distal radial cartilage in the soft portion of the dorsal fin exhibits two separate ossifications). An additional supernumerary spinous ray now articulates with the anterodorsal surface of the first proximal radial, bringing the dorsal fin formula to X-I, 25. Well-developed sculpturing is now present along the surface of the posterior groove in several of the spinous rays. All soft rays are now fully segmented but have yet to branch distally.

Comparison to C. nebulosus

The sequence of ossification for this region in the spotted seatrout is: soft rays (5.5 mm SL); spiny rays (5.7 mm SL); proximal radials (7.6 mm SL); and distal radials (13.1 mm SL).

No differences were identified between the ossification sequences for the dorsal-fin skeleton of *C. nebulosus* and *S. ocellatus*. The only difference in the adult dorsal-fin skeleton of *C. nebulosus* is that its dorsal-fin formula is X-I, 28 compared to X-I, 25 in *S. ocellatus*.

Anal Fin

I describe four different stages in the development of the anal fin. The sequence of ossification for this region is: soft rays, spiny rays (6.0 mm SL); proximal radials (7.3 mm SL); and distal radials (13.1 mm SL).

In the smallest stage illustrated (5.4 mm SL, Figure 7A), nine rod-like proximal radial cartilages and six fin rays are present. The proximal radial cartilages located towards the middle of the series are slightly longer than those located anteriorly or posteriorly in the series. The six fin rays are poorly ossified and unsegmented, and retain actinotrichia at their tips. Spinous anal-fin rays and distal radial cartilages have yet to form.

At 5.9 mm SL (Figure 7B), only eight of the original nine proximal radial cartilages are present, together with 8 small distal radial cartilages, 2 spinous dorsal-fin rays and 9 soft anal-fin rays. The anteriormost proximal radial cartilage is now much larger relative to the others and exhibits a large plate of cartilage along its anteroventral edge, which is hypothesized to be homologous with the anteriormost proximal radial cartilage present in earlier stages of development (i.e. ontogentic fusion of the two anteriormost proximal radial cartilages). All proximal radial cartilages are now associated with small spherical distal radial cartilages posteroventrally, which are in serial association with a single soft anal-fin ray, with the exception of the last, which supports the last two rays of the anal fin. Two spinous anal-fin rays are now present and in supernumerary association with the anteriormost proximal radial. The anteriomost spinous ray is represent by a pair of tiny slithers of dermal bone, which have yet to fuse across the midline, while the posteriomost is already singular. The four anteriomost soft rays have begun to segment at the midlength.

At 12.6 mm SL (Figure 7C), the anteriormost proximal radial is now almost completely ossified, with cartilage remaining only at the distal and proximal tips. The dorsalmost tip of the anteriormost proximal radial now also contacts the anteroventral edge of the first hemal spine. The remaining proximal radials are now perichondrally ossified around the midlength of the remaining proximal radial cartilages. The three anteriormost proximal radials also now exhibit well-developed lateral keels of membrane bone. The posterior proximal radial cartilage now exhibits a short posterior extension of cartilage (anal-fin stay sensu Weitzman, 1962) that extends dorsal to, and surpasses, the posteriormost distal radial cartilage. The two anteriormost distal radials are now present as two small lateral perichondral ossifications restricted to the lateral margin of their respective distal radial cartilages, adjacent to the medial face of the bases of the rays. The two spinous anal-fin rays are now much larger and extensive sculpturing is now present along the posterior groove of the posteriormost spinous ray. All nine of the soft anal-fin rays are now segmented.

At 24.1 mm SL (Figure 7D), a stage comparable to that of the adult, all pteygiophore elements now comprise a proximal and distal radial in serial association with a single soft anal-fin rays, excluding the posteriormost, which is associated with two rays, and the anteriormost, which is also in supernumerary association with the two spinous anal-fin rays. The first proximal radial now possesses a large lamina of membrane bone along most of its anterior edge. The remaining proximal radials are now well ossified, except for the distalmost tips, which remain cartilaginous. Well-developed laminae of membrane bone are now present along the anterior and posterior edges of all proximal radials and lateral keels are now present on all proximal radial elements. The anteriormost spinous anal-fin ray is also now extensively sculptured along the posterior groove of the spine. Soft rays posterior to the first are now branched distally. The anal-fin formula is II, 9.

Comparison to C. nebulosus

The sequence of ossification for this region in *C. nebulosus* is: soft rays (5.5 mm SL);

spiny rays (5.7 mm SL); proximal radials (6.8 mm SL); and distal radials (13.1 mm SL).

No differences were identified between the ossification sequences for the anal-fin skeleton of *C. nebulosus* and *S. ocellatus*. The only difference in the adult anal-fin skeleton of *C. nebulosus* is that the anal-fin formula is II, 11 compared to II, 9 in *S. ocellatus*.

Caudal Fin

I describe six different stages in the development of the caudal skeleton. The sequence of ossification for this region is: caudal-fin rays (4.8 mm NL); hypural 1 and hypural 2 (4.9 mm NL); hypural 3 (5.1 mm SL); urostyle (5.2 mm SL); hypural 4 (5.3 mm SL); preural centrum (PU) 3 (5.5 mm SL); parhypural (5.9 mm SL); PU2, hemal arch of PU3, neural arch of PU3 and hemal arch of PU2 (6 mm SL); neural arch of PU2 (6.4 mm SL); hypural 5 (6.5 mm SL); hemal spine of PU3 and hemal spine of PU2 (6.6. mm SL); neural spine of PU3 (6.8 mm SL); neural spine of PU2 (6.9 mm SL); epural 1, epural 2 and epural 3 (8.3 mm SL); uroneural 1 and uroneural 2 (9.7 mm SL).

In the smallest stage illustrated (4.1mm NL; Figure 8A), flexion has not yet taken place and the posterior tip of the notochord is surrounded by actinotrichia. Two small, round cartilages located ventral to the notochord are the only skeletal elements present. These cartilages represent hypural 1 and 2 cartilages.

At 4.5 mm NL (Figure 8B), flexion of the notochord is underway. The basidorsal and basiventral cartilages of PU 2 and 3 are present. The basiventral cartilages of the right and left sides of PU2 and 3 have already made contact across the midline to form cartilaginous hemal arches. The basidorsal cartilages of the right and left sides of PU2 and 3 have yet to make contact across the midline dorsal to the notochord. The hemal spine cartilages for PU2 and PU3 are present and represented by elongate rods of cartilage attached to the cartilaginous hemal arches. The parhypural cartilage and hypural 1-4 cartilages are well developed. Hypural 1-2 cartilages are located slightly more ventrally than hypural 3-4 cartilages. Hypural 1 cartilage is the largest of the four

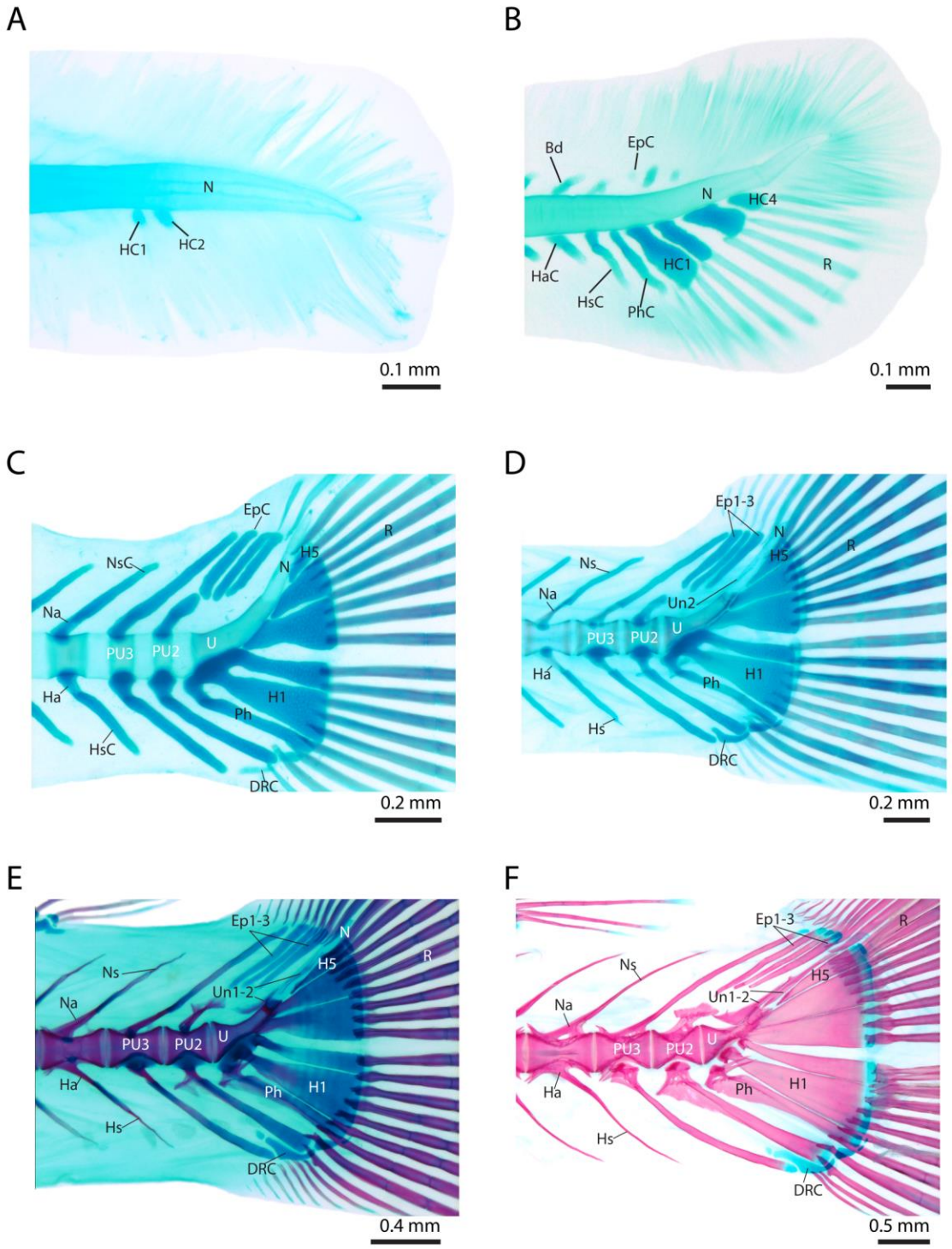

Fig. 8. Ontogeny of the caudal skeleton of *S. ocellatus* (TCWC 16420.01). **A.** 4.1 mm NL. **B.** 4.5 mm NL. **C.** 6.7 mm SL. **D.** 9.5 mm SL. **E.** 12.9 mm SL. **F.** 25.3 mm SL. DRC, Distal Radial Cartilage; Ep, Epural; EpC, Epural Cartilage; H, Hypural; HC, Hypural Cartilage; N, Notochord; Ph, Parhypural; PhC, Parhypural Cartilage; PU, Pre Ural Central; R, Soft Ray; U, Urostyle; Un, Uroneural.

hypural elements and is widest distally. Hypural 2 cartilage is more slender than hypural 1 cartilage but is similar in length. Hypural 3 cartilage is slightly shorter but approximately twice the width of hypural 2 cartilage. It is positioned more dorsally along the slightly upturned notochord than preceeding hypural elements and is separated from hypural 2 cartilage by a short diastema. Hypural 4 cartilage is situated posterodorsal to hypural 3 cartilage and is triangular in shape. Hypural 5 cartilage has yet to form. Three small epural cartilages, representing epural 1-3 cartilages, are present dorsal to notochord, directly above hypural 1-2 cartilages. At this point in development, epural 2 cartilage, located directly opposite the diastema between hypural 1 and hypural 2 cartilages, is the largest of the three epural elements. Caudal-fin rays, situated posteroventrally to the hypural cartilages, represent the only ossified structures present at this stage. Actinotrichia are still present around the posteriormost tip of the notochord.

At 6.7 mm SL (Figure 8C), flexion is now complete. PU2 and PU3 are represented by thin bands of ossification (chordacentra) around the notochord. The neural and hemal arches of PU2 and PU3 are ossified perichondrally around the midlength of the basidorsal and basiventral cartilages, respectively. Two small distal caudal radial cartilages are now present in close association with the distal tips of the hemal spine cartilages of PU3 and PU2 and the parhypural cartilage; the anteriormost between the distal tips of the hemal spine cartilages of PU3 and PU2 and posteriormost between the distal tips of the hemal spine cartilage of PU2 and the parhypural cartilage. The urocentrum is now present and represented by thin cylinder of ossification around the notochord; extending from close to the base of the parhypural cartilage to the anteriormost tip of hypural 4 cartilage. The parhypural and hypural cartilages, excluding hypural 1 cartilage, are now much larger but similar in overall shape to that of the previous stage illustrated. Hypural 1 cartilage is now much wider distally than proximally. Hypural 5 cartilage is now present as a small triangular cartilage, wedged between the ventral margin of the posterodorsally projected notochord and the dorsal margin of hypural 4 cartilage. All five hypural elements, as well as the parhypural, are ossified perichondrally around their respective cartilages. The ossifications representing

hypural 3-5 are restricted to the base of their respective cartilages, compared to the more centrally ossified hypural 1-2 or the parhypural. The proximal tip of the parhypural cartilage, hypural 1 cartilage, and hypural 2 cartilage are now continuous, forming a single cartilaginous base for all three elements. Epural 1-3 cartilages are now elongate, rod-shaped elements, situated posterior to the neural spine cartilages of PU2 and PU3. Both principal and procurrent caudal-fin rays are now present around the posterior margin of the caudal-fin endoskeleton, from the tip of PU2 hemal spine cartilage to the tip of epural 3 cartilage. There is an obvious diastema in the principal caudal-fin rays opposite the distal ends of hypural 2-3 cartilages, marking the division between the upper and lower caudal-fin lobes. Actinotrichia are no longer present.

At 9.5 mm SL (Figure 8D), PU2 and PU3 are more fully developed and have acquired the concave, cylindrical shape typical of teleost vertebral centra. The basidorsal and basiventral cartilages of PU2 and PU3 are now restricted to the very base of the neural and hemal arches, respectively. The neural spine cartilage of PU3 and the hemal spine cartilages of PU2 and PU3 now extend posterodorsally and posteroventrally, respectively, to support the bases of the procurrent caudal-fin rays. All three elements are now ossified perichondrally along their midlength and a thin flange of membrane bone is also present along the anterior edge of the hemal spine of PU2, close to the base of the spine. The neural spine cartilage of PU2 is greatly reduced compared to that of PU3 and has begun to ossify both perichondrally and endochondrally close to the distalmost tip. The two distal caudal radial cartilages described above are now much larger. The anteriormost distal caudal radial cartilage has developed a short dorsal process along its anterior edge that extends along the posterior edge of the distal tip of the hemal spine cartilage of PU3. A third distal caudal radial cartilage is now also present posterior to the distal tip of the parhypural cartilage. The urocentrum is slight longer but similar in overall shape to that described above. The hemal arch of the parhypural is now ossified and exhibits small anterior and posterior extensions of membrane bone. The parhypural as well as hypural 1 and 2 have started to ossify endochondrally along their midlength, but remain cartilaginous both distally and

proximally, including the common cartilaginous base. Hypural 3 and 4 have also begun to ossify endochondrally proximally, at the point of contact with the urocentrum. Hypural 5 cartilage has grown in size considerably, and is now more triangular in shape. A low rim of membrane bone extends along the dorsal edge of hypural 5. A small distal caudal radial cartilage, similar in size and shape to that situated posterior to the distal tip of the parhypural cartilage, is situated at the broad distal tip of hypural 5 cartilage. Uroneural 1 is present as a thin, slightly curved splint of bone resting on the posterodorsal edge of the urocentrum. Uroneural 2 is also present as a thin splint of bone along the anterodorsal edge of the notochord. Epural 1, 2 and 3 are now also present as thin perichondral ossifications around the midsection of their respective cartilages. Several additional procurrent rays are now present anterior to the principal caudal rays along the dorsal and ventral midline of the caudal skeleton.

At 12.9 mm SL (Figure 8E), PU2 is now in contact with PU3 anteriorly and the urocentrum posteriorly. The neural arches of PU2 and PU3 are now completely ossified, while small remnants of the basiventral cartilages still remain between the hemal arches and the ventral margin of these centra. A thin process of membrane bone is now present between the dorsal surface of PU3 and its neural arch and prezygapohyses have begun to form anteriorly on the dorsal and ventral surface of PU3. The neural and hemal spines of PU2 and PU3 are now ossified endochondrally. The thin extensions of membrane bone on the neural spine and hemal arch of PU2 are now much larger and have expanded considerably anteriorly. An additional, small round distal caudal radial cartilage has formed dorsal to the anterior tip of the distal caudal radial cartilage between the hemal spines of PU2 and PU3. The bases of the parhypural, hypural 1 and hypural 2 have begun to ossify endochondrally within the large common cartilaginous base connecting all three elements. A thin lamina of membrane bone is now present along the anterior edge of the parhypural, connecting the small anterior process to the main shaft of the bone. A spur-like, posterodorsally directed hypuropophysis is also now present on the posterior edge of this parhypural. Hypurals 1-5 have now taken on the shape present in the adult stage. The uroneurals are now more heavily ossified and the posterior tip of

uroneural 1 now dorsally overlaps the anterior tip of uroneural 2. All three epurals have grown considerably in length and have begun to ossify endochondrally. Additional procurrent rays have formed and now extend dorsally and ventrally to the neural and hemal spine of PU3 respectively.

At 25.3 mm SL (Figure 8F), a stage comparable to that of the adult, PU2 and PU3 are now completely formed and exhibit lateral sculpturing. A small, anterodorsally directed prezyagapophyses is now present on the anterolateral edge of PU3 but not on PU2. The neural arch of PU3 is now solidly connected to the centrum through intervening membrane bone whereas the hemal arch remains autogenous with the ventral surface of the centrum. The neural spine of PU3 and hemal spine of PU2 and PU3 are now completely ossified with the exception of the distal tips, which remain cartilaginous. The foreshortened neural spine of PU2 is now orientated horizontally. The lamina connecting the anterior extension of the hemal arch of PU2 to the anterior edge of the hemal spine has expanded posteroventrally and now terminates midway along the length of the spine. The hypuropophysis of the parhypural have extended posteriorly and now extends past the posterior edge of hypural 1. In addition to the well-developed flange of membrane bone along the anterior edge of the parahypural, a thin lamina of membrane bone is now also present along the posterodorsal edge of this bone. The cartilage connecting the heads of the parhypural, hypural 1 and hypural 2 in earlier stages is now absent and these elements now articulate independently with the ventral surface of the urocentrum. The parhypural and all five of the hypurals are now well ossified except distally, where they remain cartilaginous. The anterior half of uroneural 1 now rests along the posterodorsal edge of the urocentrum, with its posterior tip firmly connected to the dorsal surface of the anterior portion of uroneural 2. Uroneural 2 also now makes contact with the posterior tip of the urocentrum anteriorly and is closely associated with much of the dorsal margin of hypural 5. All three epurals are now well ossified, except for the distalmost tip, which remains cartilaginous. All caudal-fin rays now articulate proximally with the cartilaginous, distal tips of the supporting endoskeletal elements of the caudal skeleton.

Comparison to C. nebulosus

The sequence of ossification for this region in *C. nebulosus* is: rays; hypural 1, hypural 2, parhypural (4.7 mm NL); hypural 3 (5.3 mm SL); urostyle (5.9 mm SL); PU3, PU2 (5.9 mm SL); hypural 4, hemal arch of PU3, hemal arch of PU2, hemal spine of PU3, hemal spine of PU2 (6.1 mm SL); neural arch of PU3 (6.4 mm SL); neural arch of PU2, neural spine of PU3, neural spine of PU2 (6.5 mm SL); hypural 5 (6.6 mm SL); epural 2 (6.9 mm SL); epural 1 (7.6 mm SL); epural 3 (8.5 mm SL); uroneural 1 (9.9 mm SL); and uroneural 2 (10.3 mm SL).

The sequence of ossification for this region in *C. nebulosus* differed from that of *S. ocellatus*. In *C. nebulosus*, the parhypural develops before hypural 3 (compared to after PU3 in *S. ocellatus*) and hypural 4 develops after PU2 (compared to just after the urostyle in *S. ocellatus*). The neural arches of PU3 and PU2 develop at approximately the same size as the neural spines of these elements (compared to later than the neural arches of PU3 and PU2 in *S. ocellatus*). Hypural 5 develops after all elements of PU3 and PU2 and before the epurals (compared to earlier than the neural and hemal spines of PU3 and PU2 in *S. ocellatus*). Lastly, the epurals develop at very different lengths in *C. nebulosus*, with epural 2 developing first (compared to the epurals developing at the same time in *S. ocellatus*). Despite these differences, the adult caudal-fin skeleton of *C. nebulosus* is generally similar to that of *S. ocellatus*.

Pectoral Girdle

I describe five different stages in the development of the pectoral girdle. The sequence of ossification for this region is: cleithrum (2.5 mm NL); supracleithrum (4.0 mm NL); posttemporal (4.7 mm SL); postcleithrum 2 (4.8 mm SL); postcleithrum 1 (5.3 mm SL); pectoral-fin rays (7.3 mm SL); coracoid, scapula (7.9 mm SL); pectoral radial 1 (8.9 mm SL); pectoral radial 2 (9.6 mm SL); pectoral radial 3 (10.0 mm SL); and pectoral radial 4 (10.9 mm SL).

In the smallest stage illustrated (4.2 mm SL; Figure 9A), the cleithrum is present as a thin sliver of dermal bone, extending from a point just posterior to the neurocranium to the ventral midline, where it contacts its antimere medially. The supracleithrum is also present as a tiny splint-like bone articulating with the lateral face of the cleithrum, close to its dorsal tip. The scapulocoracoid cartilage is located posterior to the cleithrum, close to its midlength. It contacts the cleithrum via the pars scapularis, dorsally, and the pars coracoideus, ventrally, and possesses a well-developed processus coracoideus, which extends posteroventrally from the main body of the cartilage. The large, round cartilage of the pectoral radial plate abuts the posterior margin of the scapulocoracoid cartilage. It exhibits a large central incisure and is surrounded posteriorly by a field of actinotrichia.

At 5.3 mm SL (Figure 9B), the cleithrum is now much wider centrally, with the addition of a thin lamina of bone along both the anterior and posterior margin of its mid-length. The supracleithrum has retained a similar shape to the previous stage but is almost doubled in size and is now more firmly attached to the lateral surface of the cleithrum. The posttemporal is now present as a thin lamina of dermal bone that articulates medially with the lateral face of the supracleithrum dorsally. At this stage the posttemporal is composed largely of the dorsal arm, which tapers to a point anteriorly where it contacts the epioccipital. The ventral arm of the posttemporal is represented at this stage by a small process, located anteroventrally, anterior to the point of articulation with the supracleithrum. Postcleithrum 1 and 2 are now present as thin laminae of dermal bone situated medial to the scapulocoracoid cartilage and pectoral radial plate. The dorsalmost tip of postcleithrum 1 contacts the medial face of the cleithrum dorsal to the scapulocoracoid cartilage. Postcleithrum 2 is more rod-like than postcleithrum 1 and extends far beyond the chondral portion of the pectoral girdle, terminating posteroventral to the tip of the processus coracoideus of the scapulocoracoid cartilage. A large foramen, for the passage of a branch of the pterygial nerve, is now present in the pars scapularis portion of the scapulocoracoid cartilage. Two additional incisures are now present in the cartilage of the pectoral radial plate, one dorsal and one ventral to the original incisures located at the center of the plate.

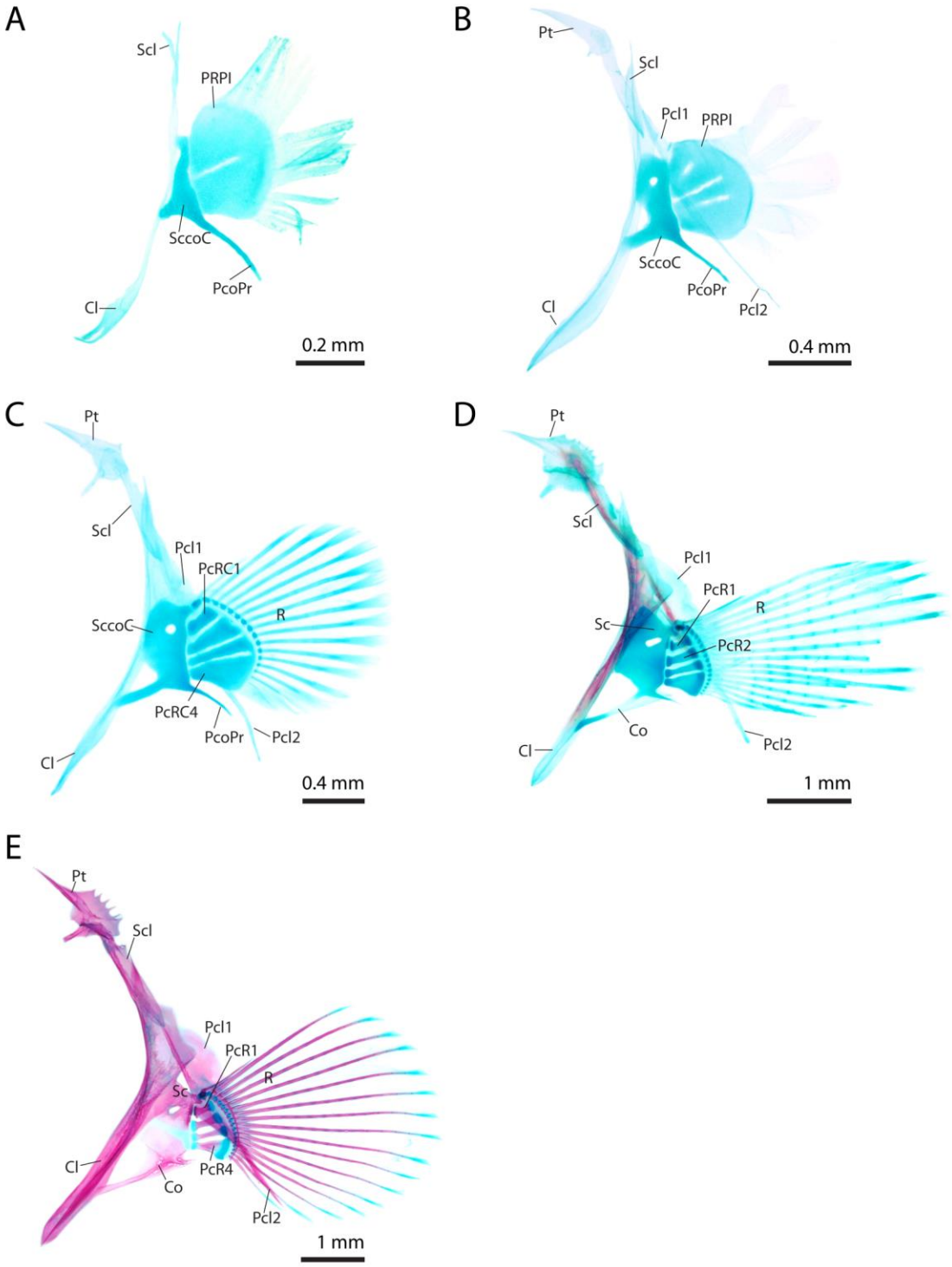

Fig. 9. Ontogeny of the pectoral girdle of *S. ocellatus* (TCWC 16420.01). **A.** 4.2 mm SL. **B.** 5.3 mm SL. **C.** 6.7 mm SL. **D.** 9.5 mm SL. **E.** 24.2 mm SL. Cl, Cleithrum; Co, Coracoid; Pcl, Postcleithrum; PcoPr, Processus Coracoideus; PcR, Pectoral Radial; PRPl, Pectoral Radial Plate; Pt, Posttemporal; R, Soft Ray; Sc, Scapula; SccoC, Scapulocoracoid Cartialge; Scl, Supracleithrum.

At 6.7 mm SL (Figure 9C), the cleithrum and supracleithrum are similar in appearance to that of the previous stage. The postemporal is now much wider posteriorly and possesses a small spine-like process along the posterodorsal edge of the bone. The ventral arm of the posttemporal is now much larger and extends far beyond the anteroventral margin of the bone. Postcleithrum 1 is now in direct contact with the posterodorsal edge of postcleithrum 2. The pars scapularis of the scapulacoracoid cartilage now possesses a posterodorsal extension, which abuts the anteroventral face of the proterygium cartilage. The processus coracoideus of the scapulacoracoid cartilage now appears shorter than in previous stages, while the anterior arm of the pars coracoideus appears to have increased in length and is now distinctly rod-shaped. The pectoral radial plate is now almost completely separated into four individual pectoral radial cartilages and small spherical distal radial cartilages are now present and rim almost the entire posterior margin of the pectoral radial cartilages, excluding the ventral margin of pectoral radial four cartilage. Pectoral-fin rays are now present but remain poorly developed with only a few exhibiting segments proximally. The bases of the hemitrichia of each ray embrace the distal radial cartilages and there is an almost one to one relationship between the number of distal radial cartilages and pectoral-fin rays. The bases of the hemitrichia of the uppermost pectoral-fin ray instead embrace the proterygium cartilage.

At 9.5 mm SL (Figure 9D), the cleithrum is now much wider posterodorsally and extensive sculpturing is now present at its mid-length. The supracleithrum is now tapered dorsally and exhibits a pronounced ridge along its lateral face. The postemporal now possesses several spine-like projections along its posterodorsal edge and exhibits a poorly ossified canal on its lateral face, which accommodates the cephalic sensory canal as it exits the neurocranium via the lateral extrascapular. The dorsal and ventral arms of the posttemporal are now tightly associated with the epioccipital and intercalar, respectively. The thin lamina of bone present on the posterior edge of postcleithrum 1 has grown considerably and its posterior margin is now curved posteriorly. Postcleithrum 2 now possesses a thin lamina of bone dorsally that medially overlaps

with the ventralmost part of postcleithrum 1. The scapula is now perichondrally ossified around the pars scapularis of the scapula coracoid cartilage and exhibits a low ridge of membrane bone along its dorsal edge. The perichondral ossification of the scapula also surrounds the posterodorsal process of the pars scapularis, which now articulates tightly around the anterior edge of the proterygium cartilage. The coracoid is now perichondrally and endochondrally ossified within the pars coracoideus of the scapulacoracoid cartilage. A well-developed flange of membrane bone extends along the posteroventral edge of the coracoid, between the anterior arm and the remnant of the processus coracoideus. The pectoral radial plate is now completely divided into four pectoral radial cartilages, with pectoral radials 1 and 2 perichondrally ossified around the mid-length of the two uppermost elements. All pectoral-fin rays are now segmented but have yet to branch distally. The base of the outer hemitrichium of the uppermost pectoral-fin ray is now greatly enlarged compared to that of other rays.

At 24.2 mm SL (Figure 9E), a stage comparable to that of the adult, all dermal elements (excluding the pectoral-fin rays) now exhibit extensive sculpturing. The cleithrum now possesses a well-developed lateral keel along its ventral limb. The dorsal tip of the supracleithrum is now spine-like and orientated anterodorsally. The spines-like processes along the posterodorsal edge of the posttemporal are now more pronounced and the tip of the ventral arm is now rounded and no longer tapers to a fine point, as is the case in the dorsal arm. The anteroventral tip of postcleithrum 1 is now fused with the dorsal edge of postcleithrum 2, forming a single rod-like element medial to the pectoral radials. The scapular and the coracoid are now completely ossified but remain separated by a thin strip of cartilage, a remnant of the scapulocoracoid cartilage. All four pectoral radials are now ossified endochondrally but all retain remnants of the precausory pectoral radial cartilages at both ends, except for the anterior edge of pectoral radial 1, which articulates tightly with the posterior edge of the scapula, directly ventral to the posterodorsal process. The pectoral-fin rays are now fully developed but have yet to branch distally. The proterygium cartilage is now ossified endochondrally and the base

of the outer hemitrichium of the uppermost pectoral-fin ray now surrounds the entire lateral face of this element.

Comparison to C. nebulosus

The sequence of ossification for this region in the spotted seatrout is: cleithrum (2.6 mm NL); supracleithrum (3.7 mm NL); posttemporal (3.8 mm NL); postcleithrum 2 (4.7 mm NL); postcleithrum 1 (5.5 mm SL); coracoid (6.9 mm SL); fin rays, scapula (7.6 mm SL); pectoral-radial 1 (9.5 mm SL); pectoral-radial 2 (9.9 mm SL); pectoral-radial 3 (10.3 mm SL); and pectoral-radial 4 (11.5 mm SL).

The sequence of ossification for this region in *C. nebulosus* is very similar to that of *S. ocellatus*, differing only in one aspect. In *C. nebulosus*, the coracoid develops before the pectoral-fin rays (compared to after the pectoral-fin rays in *S. ocellatus*). The only difference in the adult pectoral-fin skeleton of *C. nebulosus* is that it has 17 fin rays compared to 18 in *S. ocellatus*.

Pelvic Girdle

I describe four stages in the development of the pelvic girdle. The sequence of ossification for this region is: spiny ray, soft rays and basipterygium (8.3 mm SL).

In the smallest stage illustrated (8.2 mm SL; Figure 10A), the basipterygia are represented by a pair of small rod shaped cartilages, which are widest posteriorly. The pelvic-fin spine is already present at this stage, together with three poorly developed pelvic-fin rays. All four of these exoskeletal elements articulate directly with the posterior edge of the basipterygium cartilage.

At 9.2 mm SL (Figure 10B), the basipterygia cartilages are now much larger and are situated closer to the ventral midline but remain separate. The basipterygium has started to ossify perichondrally around the anteriormost tip of the basipterygium cartilage. The posteriormost tip of the basipterygium cartilage has developed a short medially directed extension. A small round pelvic radial cartilage has developed close to the posteromedial

Fig. 10. Ontogeny of the pelvic girdle of *S. ocellatus* (TCWC 16420.01). **A.** 8.2 mm SL. **B.** 9.2 mm SL. **C.** 12.6 mm SL. **D.** 24.1 mm SL. Bp, Basypterigium; BpC, Basypterygium Cartilage; PlvRC, Pelvic Radial Cartilage; R, Soft Ray; S, Spiny Ray.

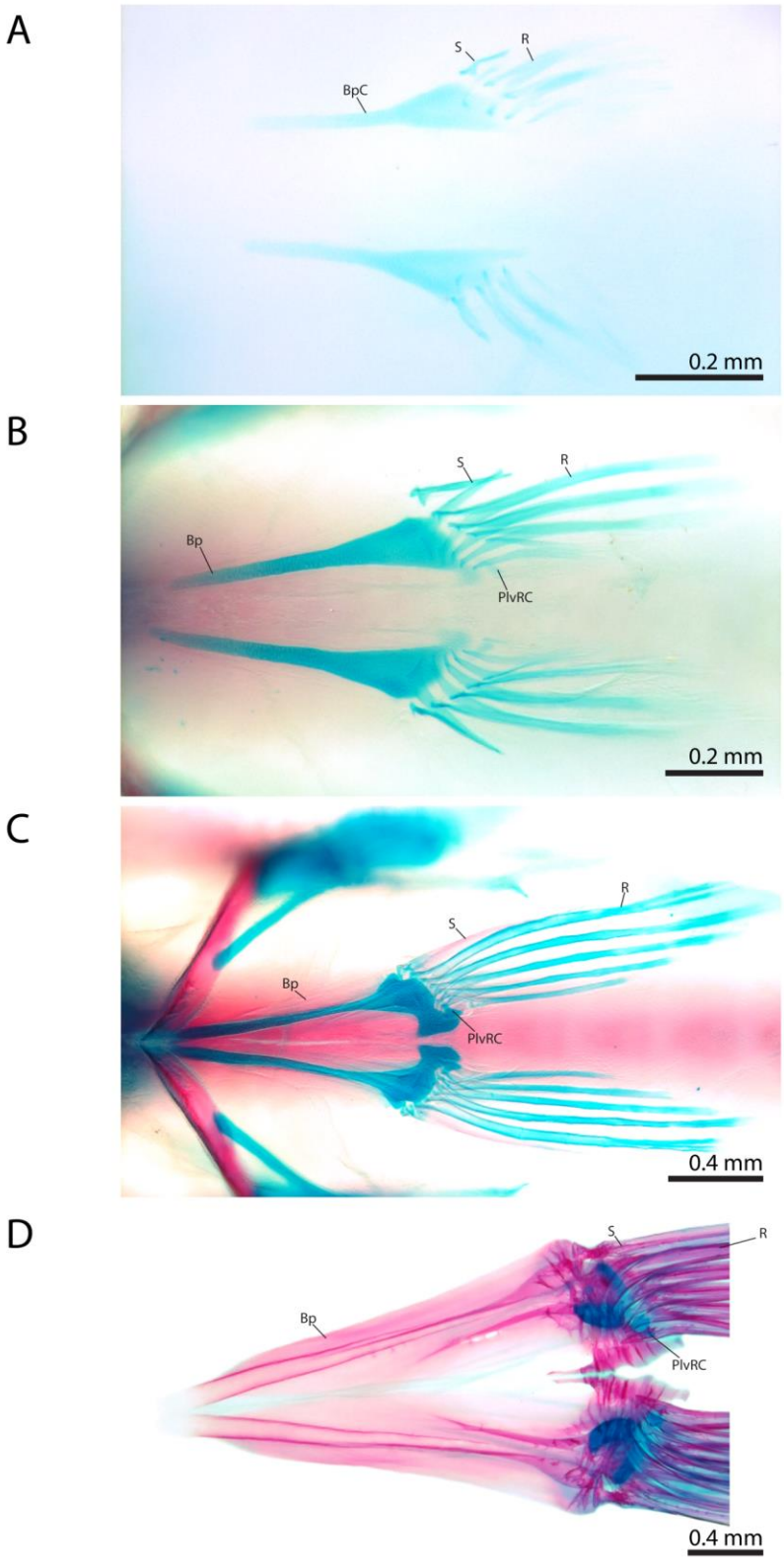
A
S
R
BpC
0.2 mm
B
S
R
Bp
PlvRC
0.2 mm
C
R
S
Bp
PlvRC
0.4 mm
D
S
R
Bp
PlvRC
0.4 mm

tip of the basipterygium cartilage. The pelvic-fin spine and pelvic-fin rays are now more heavily ossified but the individual hemitrichia of the pelvic-fin rays are not yet segmented. A fourth pelvic-fin ray is now present medial to the third.

At 12.6 mm SL (Figure 10C), the anterior tips of the basipterygia are now in direct contact with the cleithra of the pectoral girdle. The basipterygium now exhibits a thin flange of membrane bone along both lateral and medial edges, giving the element a more triangular appearance. The posteromedial extension of the basipterygium cartilage is now considerably larger and has extended posteriorly to rim the entire medial edge of the adjacent pelvic radial cartilage. The articulatory head of the pelvic-fin spine is now much larger and more heavily ossified than the heads of other pelvic-fin lepidotrichia. Segments are now present in the hemitrichia of the three outermost pelvic-fin rays and the outermost ray is now branched distally. A fifth pelvic-fin ray is now present, articulating directly with the pelvic radial cartilage.

At 24.1 mm SL (Figure 10D), a stage comparable to that of the adult, most of the basipterygium cartilage has been replaced by bone, except for an irregularly shaped block of cartilage along the posterior margin of the basipterygium. A ventral keel is also now present along the ventral midline of the basypterigium and extensive sculpturing covers the ventral surface of the posterior region of the bone. The head of the pelvic spine also exhibits sculpturing. The posteromedial extension of the basipterygium is now tightly sutured with its antimere across the ventral midline, forming a tight connection between the basipterygia. The two innermost rays are now segmented and all rays are now branched distally.

Comparison to C. nebulosus

The sequence of ossification for this region in the spotted seatrout is: spiny ray, soft rays and basypterigium (7.6 mm SL).

No differences were identified between the ossification sequences for the pelvic-fin skeleton of *C. nebulosus* and *S. ocellatus*. The adult pelvic-fin skeleton of *C. nebulosus* is generally similar to that of *S. ocellatus*.

DISCUSSION

Skeletal Development in *Sciaenops ocellatus* and *Cynocion nebulosus*

Skeletal development in both *Sciaenops ocellatus* and *Cynocion nebulosus* occurs rapidly, with all bony elements (excluding the basisphenoid and the sclerotic bones) present by 14.4 mm SL and 13.5 mm SL, respectively (Figure 11 and 12). The basisphenoid did not begin to appear until 17.1 mm SL (fixed by 21.9 mm SL) in the sampled series of *S. ocellatus* or until 16.0 mm SL (fixed by 19.5 mm SL) in the sampled series of *C. nebulosus*, leaving a gap of 10.5 mm and 7.5 mm, respectively, between the development of the basisphenoid and the extrascapulars and dermosphenotic, the penultimate elements in the development of the neurocranium in both species. The sclerotic bones, which are present in the adult stage of both *S. ocellatus* (Topp and Cole, 1968) and *C. nebulosus* (pers. obs; TCWC 11202.23), were absent in all individuals of the developmental series of each species compiled for this study, suggesting that these elements form much later in development, at sizes beyond that of the material sampled herein. Overall, the skeleton developed slightly faster in *C. nebulosus* than in *S. ocellatus*. This is not surprising as it is generally observed that smaller species tend to develop quicker than larger bodied, closely related species; a concept first proposed by Reiss (1989) and observed in the skeletal development of *Puntius semifasciolatus* by Block and Mabee (2012). Despite the difference in overall size at first appearance of skeletal elements between *C. nebulosus* and *S. ocellatus*, no major differences were found between the sequences of ossification for the two species by region (Figures 11 and 12) other than relatively minor differences involving the switching of one or two bones in the order of the sequence (see comparisons between ossification sequence of *S. ocellatus* and *C. nebulosus* in results section).

Surprisingly, despite the large number of specimens of *S. ocellatus* examined (n=237; including 145 double stained and 95 single stained), I encountered no obvious individual (asymmetry) or intraspecific (between individual) variation in the presence/absence of skeletal elements for this species. Low levels of individual and intraspecific variation

Fig. 11. Ossification sequence of 149 skeletal elements of *Sciaenops ocellatus*. Black bars represent the length of fixation. Error bars indicate length of appearance is some but not all individuals. Vertical axis equal length in mm NL/SL.

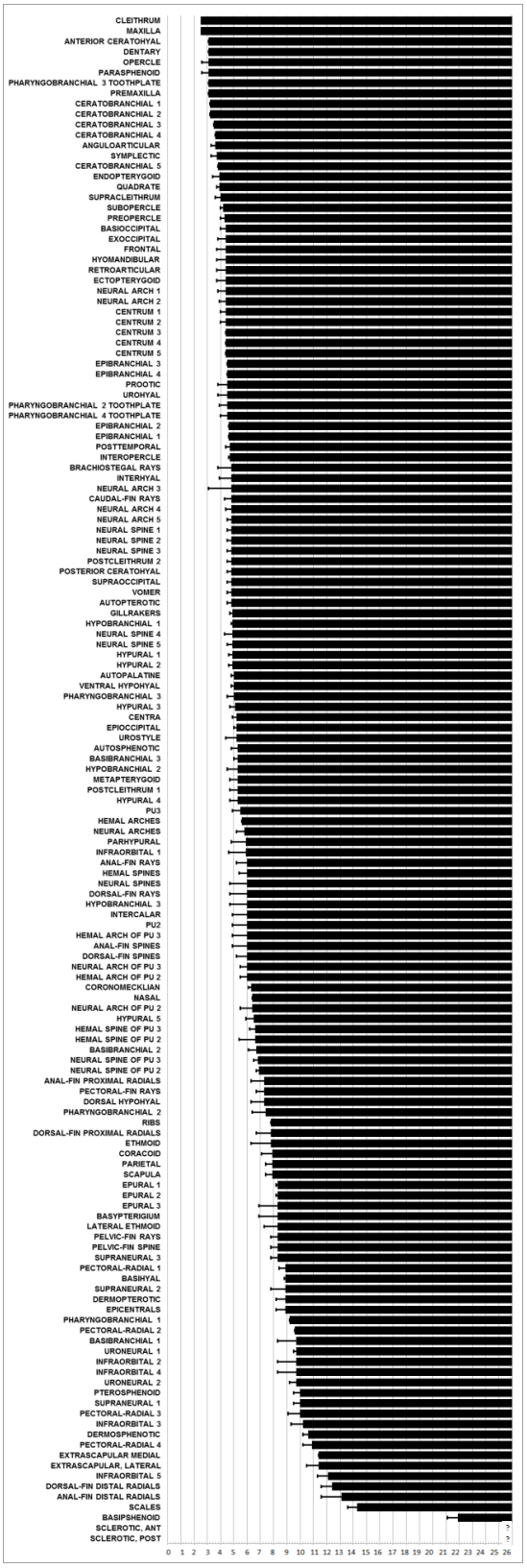
CLEITHRUM
MAXILLA
ANTERIOR CERATOHYAL
DENTARY
OPERCLE
PARASPHENOID
PHARYNGOBRANCHIAL 3 TOOTHPLATE
PREMAXILLA
CERATOBRANCHIAL 1
CERATOBRANCHIAL 2
CERATOBRANCHIAL 3
CERATOBRANCHIAL 4
ANGULOARTICULAR
SYMPLECTIC
CERATOBRANCHIAL 5
ENDOPTERYGOID
QUADRATE
SUPRACLEITHRUM
SUBOPERCLE
PREOPERCLE
BASIOCCIPITAL
EXOCCIPITAL
FRONTAL
HYOMANDIBULAR
RETROARTICULAR
ECTOPTERYGOID
NEURAL ARCH 1
NEURAL ARCH 2
CENTRUM 1
CENTRUM 2
CENTRUM 3
CENTRUM 4
CENTRUM 5
EPIBRANCHIAL 3
EPIBRANCHIAL 4
PROOTIC
UROHYAL
PHARYNGOBRANCHIAL 2 TOOTHPLATE
PHARYNGOBRANCHIAL 4 TOOTHPLATE
EPIBRANCHIAL 2
EPIBRANCHIAL 1
POSTTEMPORAL
INTEROPERCLE
BRACHIOSTEGAL RAYS
INTERHYAL
NEURAL ARCH 3
CAUDAL-FIN RAYS
NEURAL ARCH 4
NEURAL ARCH 5
NEURAL SPINE 1
NEURAL SPINE 2
NEURAL SPINE 3
POSTCLEITHRUM 2
POSTERIOR CERATOHYAL
SUPRAOCCIPITAL
VOMER
AUTOPTEROTIC
GILLRAKERS
HYPOBRANCHIAL 1
NEURAL SPINE 4
NEURAL SPINE 5
HYPURAL 1
HYPURAL 2
AUTOPALATINE
VENTRAL HYPOHYAL
PHARYNGOBRANCHIAL 3
HYPURAL 3
CENTRA
EPIOCCIPITAL
UROSTYLE
AUTOSPHENOTIC
BASIBRANCHIAL 3
HYPOBRANCHIAL 2
METAPTERYGOID
POSTCLEITHRUM 1
HYPURAL 4
PU3
HEMAL ARCHES
NEURAL ARCHES
PARHYPURAL
INFRAORBITAL 1
ANAL-FIN RAYS
HEMAL SPINES
NEURAL SPINES
DORSAL-FIN RAYS
HYPOBRANCHIAL 3
INTERCALAR
PU2
HEMAL ARCH OF PU 3
ANAL-FIN SPINES
DORSAL-FIN SPINES
NEURAL ARCH OF PU 3
HEMAL ARCH OF PU 2
CORONOMECKLIAN
NASAL
NEURAL ARCH OF PU 2
HYPURAL 5
HEMAL SPINE OF PU 3
HEMAL SPINE OF PU 2
BASIBRANCHIAL 2
NEURAL SPINE OF PU 3
NEURAL SPINE OF PU 2
ANAL-FIN PROXIMAL RADIALS
PECTORAL-FIN RAYS
DORSAL HYPOHYAL
PHARYNGOBRANCHIAL 2
RIBS
DORSAL-FIN PROXIMAL RADIALS
ETHMOID
CORACOID
PARIETAL
SCAPULA
EPURAL 1
EPURAL 2
EPURAL 3
BASYPTERIGIUM
LATERAL ETHMOID
PELVIC-FIN RAYS
PELVIC-FIN SPINE
SUPRANEURAL 3
PECTORAL-RADIAL 1
BASIHYAL
SUPRANEURAL 2
DERMOPTEROTIC
EPICENTRALS
PHARYNGOBRANCHIAL 1
PECTORAL-RADIAL 2
BASIBRANCHIAL 1
URONEURAL 1
INFRAORBITAL 2
INFRAORBITAL 4
URONEURAL 2
PTEROSPHENOID
SUPRANEURAL 1
PECTORAL-RADIAL 3
INFRAORBITAL 3
DERMOSPHENOTIC
PECTORAL-RADIAL 4
EXTRASCAPULAR MEDIAL
EXTRASCAPULAR, LATERAL
INFRAORBITAL 5
DORSAL-FIN DISTAL RADIALS
ANAL-FIN DISTAL RADIALS
SCALES
BASIPSHENOID
SCLEROTIC, ANT
SCLEROTIC, POST
?
?
0 1 2 3 4 5 6 7 8 9 10 11 12 13 14 15 16 17 18 19 20 21 22 23 24 25 26

Fig. 12. Ossification sequence of 149 skeletal elements of *Cynoscion nebulosus*. Black bars represent the length of fixation. Error bars indicate length of appearance is some but not all individuals. Vertical axis equal length in mm NL/SL.

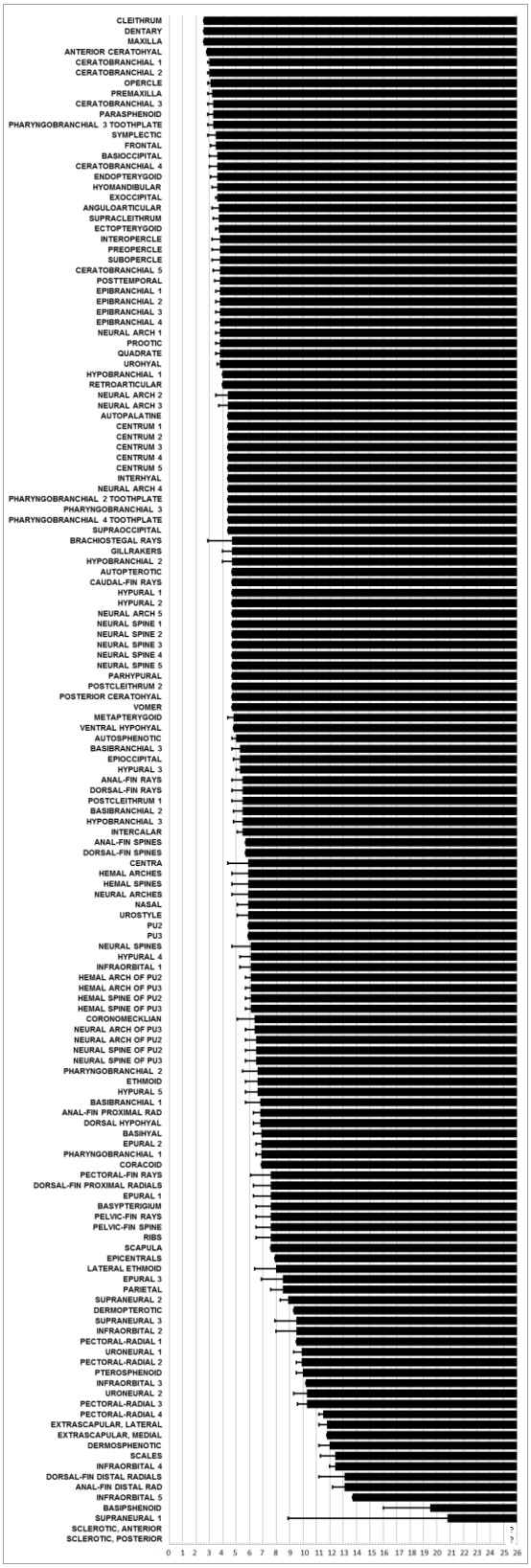
CLEITHRUM
DENTARY
MAXILLA
ANTERIOR CERATOHYAL
CERATOBRANCHIAL 1
CERATOBRANCHIAL 2
OPERCLE
PREMAXILLA
CERATOBRANCHIAL 3
PARASPHENOID
PHARYNGOBRANCHIAL 3 TOOTHPLATE
SYMPLECTIC
FRONTAL
BASIOCCIPITAL
CERATOBRANCHIAL 4
ENDOPTERYGOID
HYOMANDIBULAR
EXOCCIPITAL
ANGULOARTICULAR
SUPRACLEITHRUM
ECTOPTERYGOID
INTEROPERCLE
PREOPERCLE
SUBOPERCLE
CERATOBRANCHIAL 5
POSTTEMPORAL
EPIBRANCHIAL 1
EPIBRANCHIAL 2
EPIBRANCHIAL 3
EPIBRANCHIAL 4
NEURAL ARCH 1
PROOTIC
QUADRATE
UROHYAL
HYPOBRANCHIAL 1
RETROARTICULAR
NEURAL ARCH 2
NEURAL ARCH 3
AUTOPALATINE
CENTRUM 1
CENTRUM 2
CENTRUM 3
CENTRUM 4
CENTRUM 5
INTERHYAL
NEURAL ARCH 4
PHARYNGOBRANCHIAL 2 TOOTHPLATE
PHARYNGOBRANCHIAL 3
PHARYNGOBRANCHIAL 4 TOOTHPLATE
SUPRAOCCIPITAL
BRACHIOSTEGAL RAYS
GILLRAKERS
HYPOBRANCHIAL 2
AUTOPTEROTIC
CAUDAL-FIN RAYS
HYPURAL 1
HYPURAL 2
NEURAL ARCH 5
NEURAL SPINE 1
NEURAL SPINE 2
NEURAL SPINE 3
NEURAL SPINE 4
NEURAL SPINE 5
PARHYPURAL
POSTCLEITHRUM 2
POSTERIOR CERATOHYAL
VOMER
METAPTERYGOID
VENTRAL HYPOHYAL
AUTOSPHENOTIC
BASIBRANCHIAL 3
EPIOCCIPITAL
HYPURAL 3
ANAL-FIN RAYS
DORSAL-FIN RAYS
POSTCLEITHRUM 1
BASIBRANCHIAL 2
HYPOBRANCHIAL 3
INTERCALAR
ANAL-FIN SPINES
DORSAL-FIN SPINES
CENTRA
HEMAL ARCHES
HEMAL SPINES
NEURAL ARCHES
NASAL
UROSTYLE
PU2
PU3
NEURAL SPINES
HYPURAL 4
INFRAORBITAL 1
HEMAL ARCH OF PU2
HEMAL ARCH OF PU3
HEMAL SPINE OF PU2
HEMAL SPINE OF PU3
CORONOMECKLIAN
NEURAL ARCH OF PU3
NEURAL ARCH OF PU2
NEURAL SPINE OF PU2
NEURAL SPINE OF PU3
PHARYNGOBRANCHIAL 2
ETHMOID
HYPURAL 5
BASIBRANCHIAL 1
ANAL-FIN PROXIMAL RAD
DORSAL HYPOHYAL
BASIHYAL
EPURAL 2
PHARYNGOBRANCHIAL 1
CORACOID
PECTORAL-FIN RAYS
DORSAL-FIN PROXIMAL RADIALS
EPURAL 1
BASYPTERIGIUM
PELVIC-FIN RAYS
PELVIC-FIN SPINE
RIBS
SCAPULA
EPICENTRALS
LATERAL ETHMOID
EPURAL 3
PARIETAL
SUPRANEURAL 2
DERMOPTEROTIC
SUPRANEURAL 3
INFRAORBITAL 2
PECTORAL-RADIAL 1
URONEURAL 1
PECTORAL-RADIAL 2
PTEROSPHENOID
INFRAORBITAL 3
URONEURAL 2
PECTORAL-RADIAL 3
PECTORAL-RADIAL 4
EXTRASCAPULAR, LATERAL
EXTRASCAPULAR, MEDIAL
DERMOSPHENOTIC
SCALES
INFRAORBITAL 4
DORSAL-FIN DISTAL RADIALS
ANAL-FIN DISTAL RAD
INFRAORBITAL 5
BASIPSHENOID
SUPRANEURAL 1
SCLEROTIC, ANTERIOR
SCLEROTIC, POSTERIOR
? ?
0 1 2 3 4 5 6 7 8 9 10 11 12 13 14 15 16 17 18 19 20 21 22 23 24 25 26

were, however, observed for two skeletal elements (coronomeckelian and supraneural 1) in the material of *C. nebulosus* examined (n=214; including 133 double stained and 81 single stained). In the sampled material of *C. nebulosus*, the coronomeckelian typically developed by 6.4 mm SL, but failed to develop (i.e., absent) by this size in one of the 214 individuals examined and was present by this size only on one side (either right or left side) of the lower jaw in 20 of the 213 individuals in which this ossification developed. Both variation in the presence/absence of supraneural 1 cartilage and the subsequent ossification of this element was identified. In the sampled material of *C. nebulosus*, supraneural 1 typically ossified by 8.9 mm SL but failed to ossify by this size in 41 out of the 214 individuals examined and in another 41 individuals supraneural 1 cartilage was completely absent.

The intraspecific variation observed for supraneural 1 in *C. nebulosus* may have broader significance for the phylogenetic relationships of sciaenids. In his monographic investigation of the musculoskeletal system of sciaenids, Sasaki (1989) considered the presence of three supraneurals (= predorsals of Sasaki) to be a plesiomorphic condition at the level of Sciaenidae, with various levels of reduction providing support for less inclusive groups within Sciaenidae. In particular, Sasaki (1989) considered the absence of supraneural 1 (his character 98; "predorsals number less than three – *Cynoscion* type") to represent a synapomorphy uniting the genera *Cynoscion*, *Macrodon* and *Isopisthus*. Given that three different conditions for supraneural 1 are present within the material of *C. nebulosus* examined as part of this study ([1] supraneural 1 present; [2] supraneural 1 absent but supraneural 1 cartilage present; and [3] both supraneural 1 and supraneural 1 cartilage absent; Fig. 7), the validity of Sasaki's character 98 as evidence supporting a close relationship between *Cynoscion* and other genera that are considered to lack this element (*Macrodon* and *Isopisthus*) should be reevaluated.

Comparison with Development in Other Sciaenids

Though information on skeletal development in sciaenids is limited, two previous studies have investigated aspects of skeletal development in members of the Sciaenidae

(Jardim and Santos, 1994; Cardeira et al., 2012) that provide an opportunity to make general comparisons across the family.

Cardeira et al. (2012) investigated development of the axial skeleton in the Meagre, *Argyrosomus regius*, based on approximately 500 hatchery raised individuals. Based on their data, development of the vertebral column and median fins in *A. regius* is very similar to that reported herein for *S. ocellatus* and *C. nebulosus*, with only one notable difference regarding the formation of centra. In *A. regius*, centra 5-24 are reported to form from two separate ossification centers, one each around the dorsal and ventral margins of the notochord, which meet laterally later in development to form a complete ring of ossification (chordocentra) around the notochord. In the sampled material of *S. ocellatus* and *C. nebulosus*, only a single center of ossification, located around the ventral margin of the notochord, was observed during early centra formation. Interestingly, in all three species centra 1-4 begin to ossify close to the bases of their respective neural arches and develop in a ventral direction, forming saddle-like ossifications around the notochord prior to centra completion. Development of the four anteriormost centra appears to be highly variable across the limited number of perciforms for which developmental data on these elements is available. In the common snook (*Centropomus undecimalis*), saddle-like ossifications were only observed in the development of the first two centra (Potthoff and Tellock, 1983), while both dorsal and ventral saddle-like ossifications were observed in the development of centra 1-4 in the members of the Gempylidae and Scombridae investigated by Potthoff et al. (1986). In the genus *Morone*, saddle-like ossfications were not observed and centra are reported to ossify as complete rings around the notochord (Fritzche and Johnson, 1980). The consistency with which centra 1-4 develop in the three species of sciaenids for which developmental data for these elements are available may be indicative of a conserved pattern within the Sciaenidae. Additional data on the development of the vertebral column across percomorphs are needed.

Jardim and Santos (1994) investigated development of the neurocranium in the Whitemouth croaker, *Micropogonias furnieri,* based on 60 wild caught individuals. Based on their data, a number of differences are apparent between the development of the neurocranium in *M. furnieri* and that reported herein for *S. ocellatus* and *C. nebulosus*. Firstly, the neurocranium of *M. furnieri* appears to develop at a much slower rate than that of *S. ocellatus* and *C. nebulosus*. Jardim and Santos (1994) consider development of the neurocranium to be complete at approximately 35 mm SL, which corresponds with the appearance of the nasal and the pterosphenoid, the two last bones reported to develop in *M. furnieri*. In *S. ocellatus* and *C. nebulosus*, development of the neurocranium, excluding the basisphenoid, was complete by 11.4 and 12.0 mm SL, respectively. In both species, the nasal and pterosphenoid appear towards the middle of the sequence of ossification for the neurocranium, appearing at 6.4 and 10.0 mm SL, respectively, in *S. ocellatus*, and 5.9 and 10.0 mm SL, respectively, in *C. nebulosus*. Contrastingly, three other bones (the supraoccipital, dermopterotic, and basisphenoid) appear relatively early in the sequence of ossification for the neurocranium of *M. furnieri* compiled by Jardim and Santos (1994) when compared to their position in the sequence of ossification for the neurocranium of *S. ocellatus* and *C. nebulosus.* If the data from Jardim and Santos (1994) are comparable with the data collected herein, notable differences may exist in neurocranium development across Sciaenidae but more information on the development of other sciaenid species are needed before meaningful conclusions are reached.

Comparison with Other Teleosts

Studies on the progression of skeletal development in teleost fishes typically focus only on a specific region of the skeleton (e.g., the cranial or postcranial skeleton) and information on the sequence of ossification for the entire skeleton is currently available only for one other teleost, the Zebrafish, *Danio rerio* (Cubbage and Mabee, 1996; Bird and Mabee, 2003; Britz & Conway, 2009). Though sciaenids and cyprinids are not close relatives, I was interested to compare the data collected herein with that available for *D.*

rerio. Several skeletal elements present in *Danio rerio* are not present in sciaenids (and vice versa) and only those elements present in both taxa were compared. For the sake of simplicity only the sequence of ossification compiled for *S. ocellatus* was used in the comparison.

Surprisingly, ossification sequences compiled by region for each of the two species were strikingly similar, with only four major differences apparent. In the neurocranium, the pterosphenoid and the lateral ethmoid appear relatively early in the sequence of ossification for *D. rerio*, while they were two of the last bones to develop within the neurocranium of *S. ocellatus*. In the hyopalatine arch, the symplectic was one of the earliest bones to develop in this region for *S. ocellatus* but was one of the last to appear in *D. rerio*. Finally, the order of ceratobranchial formation in *S. ocellatus* was reversed compared to that of *D. rerio*. In *D. rerio*, ceratobranchial 5 was the first ossification of the gill arches to develop, followed shortly by ceratobranchial 4 and then ceratobranchials 1-3 (Cubbage and Mabee, 1996). In *S. ocellatus*, ceratobranchial 1 is the first ceratorbranchial element to ossify, followed by ceratobranchials 2-4, then ceratobranchial 5. Ceratobranchial 5 is highly modified in *D. rerio* and the pharyngeal teeth ankylosed to its surface represent the only teeth present in this and other cypriniform fishes (Fink and Fink, 1981). The early appearance of ceratobranchial 5 in *D. rerio* (and other cyprinform fishes studied to date; Vandewelle et al., 1992; Engeman et al., 2009; Block and Mabee, 2012; Engeman and Mabee, 2012) may be indicative of the significance of this element to the biology of cyprinform fishes in general.

Arratia and Bagarinao (2010) compared development of the cranium in the Milkfish (*Chanos chanos*) with that of *D. rerio* and reported a number of differences. Given the minor differences that exist between cranial development of *D. rerio* and *S. ocellatus*, I was interested to compare development of the neurocranium in *Chanos chanos* with that of *S. ocellatus*. This comparison revealed 14 differences in the sequence of ossification for the cranial skeleton. In the ethmoid region of the neurocranium of *C. chanos*, the lateral ethmoid is the second ossification to appear while the nasals are the last to appear

in the region (Table 1). This is switched in *S. ocellatus,* with the nasals being the second ossification to appear while the lateral ethmoids appear last in the region. In the orbital region, the pterosphenoid, despite being one of the later bones to develop in *S. ocellatus,* develops much earlier, directly after the parasphenoid, in *C. chanos*. In the otic region, the epioccipital and the parietal develop later in *C. chanos,* compared to relatively early in *S. ocellatus,* while the lateral extrascapular, one of the very last bones to develop in *S. ocellatus,* develops much earlier in *C. chanos*. In the hyopalatine arch, the ectopterygoid, coronomeckelian and metapterygoid develop early in *C. chanos* compared to late in *S. ocellatus*. Additionally, the maxilla and anterior ceratohyal develop much later in *C. chanos* despite being some of the first bones to develop in *S. ocellatus*. The angular and articular appear at different sizes in *C. chanos* and much larger sizes (SL) than in the material of *S. ocellatus* examined herein. Finally, in the gill arches, pharyngobranchial 3 develops late in *C. chanos* compared to early in *S. ocellatus*. These differences along with several other variations of ossification sequences available for the cranial skeleton (Faustino and Power, 2001) suggests that high amounts of variation exist for skeletal development in fishes and that the high similarity between the ossifications sequences available for *S. ocellatus* and *D. rerio* may be coincidental. This reinforces the idea that more studies of this nature are required.

Implications for Captive Propogation

Over the last two decades there has been a global effort to diversify the species of fishes that are targeted by aquaculture (FAO, 2012). Consequently, the numbers of studies documenting skeletal development in fishes that are raised commercially (Koumoundouros et al., 1997; Lewis-McCrea and Lall, 2007) or have been proposed as candidate species for aquaculture (Koumoundouros et al., 2000, 2001; Cardeira et al. 2012) have also increased. Such studies aim to enhance the captive propagation of their focal species by facilitating the identification of skeletal malformations (Koumoundouros et al., 1997; Cardeira et al. 2012; Tong et al., 2012), which are often the only indication that problems have occurred during the rearing process. Given the

Table 1. Sequence of ossification of nine cranial regions in *Sciaenops ocellatus* and comparison with *Danio rerio* and *Chanos chanos* (after Arratia and Bagarinao, 2010; Cubbage and Mabee, 1996). Names in bold represent elements that show differences when compared to *S. ocellatus*. The vertical arrangement follows the sequence of ossification of bones in each cranial region.

	Sciaenops ocellatus	***Danio rerio***	***Chanos chanos***
Olfactory	Vomer	**Lateral ethmoid**	Vomer
	Nasal	Vomer	**Lateral Ethmoid**
	Ethmoid	Nasal	Mesethmoid
	Lateral Ethmoid	Ethmoid	**Nasal**
Orbital	Parasphenoid	Parasphenoid	Parasphenoid
	Frontal	**Pterospenoid**	**Pterosphenoid**
	Infraorbital 1	Infraorbital 1	Frontal and
	Infraorbital 2 and	Frontal	Infraorbital 1
	Infraorbital 4	Anterior Sclerotic and	Infraorbital 4
	Pterosphenoid	Posterior Sclerotic and	Infraorbital 2
	Dermosphenotic	Dermosphenotic and	Infraorbital 3
	Infraorbital 3	Infraorbital 3	Dermosphenotic
	Anterior Sclerotic	Infraorbital 4	
	Posterior Sclerotic	Infraorbital 2	
Otic	Prootic	Prootic	Prootic and
	Posttemporal	Posttemporal	Posttemporal
	Autopterotic	Pterotic	Pterotic and
	Epioccipital	Sphenotic	**Lateral Extrascapular**
	Autosphenotic	Parietal	Autosphenotic
	Intercalar	Epioccipital	Entercalar
	Parietal	Intercalar and	**Epioccipital**
	Dermopterotic	Extrascapular	Medial Extrascapula
	Lateral Extrascapular		**Parietal**
	Medial Extrascapular		
Occipital	Basioccipital and	Exoccipital	Basioccipital and
	Exocippital	Basioccipital	Exoccippital
Mandibular Arch	**Maxilla**	Endopterygoid and	Dentary and
	Dentary and	Maxilla and	Ectopterygoid and
	Premaxilla	Dentary	Quadrate
	Anguloarticular	Quadrate	**Coronomeckelian** and

Table 1. Continued

	Sciaenops ocellatus	*Danio rerio*	*Chanos chanos*
Mandibular Arch Cont.	Endopterygoid and Quadrate Retroarticular and **Ectopterygoid** Autopalatine **Metapterygoid** **Coronomecklian**	Retroarticular and Anguloarticular Premaxilla Ectopterygoid Coronomecklian Metapterygoid Autopalatine	**Maxilla** and Premaxilla and **Metapterygoid** and Endopterygoid **Angular** and Retroarticular Autopalatine **Articular**
Hyoid Arch	**Anterior Ceratohyal** **Symplectic** Hyomandibula Urohyal Branchiostegal Rays and Posterior Ceratohyal Ventral Hypohyal Dorsal Hypohyal Basihyal	Branchiostegal Rays Hyomadibula and Urohyal Anterior Ceratohyal and Ventral Hypohyal Posterior Ceratohyal and **Symplectic** Basihyal Dorsal Hypohyal	Hyomandibula Urohyal Branchiostegal Rays Symplectic Ventral Hypohyal **Anterior Ceratohyal** Posterior Ceratohyal Dorsal Hypohyal Basihyal
Opercular	Opercle Subopercle Preopercle Interopercle	Opercle Interopercle and Subopercle Preopercle	Opercle Subopercle Preopercle Interopercle
Branchial Arches	**Ceratobranchials 1-2** **Ceratobranchial 3** **Ceratobranchial 4** **Ceratobranchial 5** eEpibranchials 3-4 Epibranchials 1-2 Hypobranchial 1 **Pharyngobranchial 3** Basibranchial 3 and Hypobranchial 2	**Ceratobranchial 5** Epibranchial 4 **Ceratobranchial 4** Epibranchial 3 **Ceratobranchial 1-3 and** Epibranchials 1-2 Pharyngobranchial 2+3 Basibranchial 1-3 Hypobranchial 3 Pharyngobranchial 1	Ceratobranchials 1-5 and Epibranchials 1-4 and Basibranchials 2-3 and Hypobranchial 1 Hypobranchial 2 Pharyngobranchial 2 **Pharyngobranchial 3** Hypobranchial 3 Basibranchial 1 Pharyngobranchial 1

Table 1 Continued

	Sciaenops ocellatus	*Danio rerio*	*Chanos chanos*
Branchial Arches Cont.	Hypobranchial 3 Basibranchial 2 Pharyngobranchial 2 Pharyngobrancial 1 Basibranchial 1	Hypobranchial 2 Hypobranchial 1 if ossified	

direct advantages of having information on normal skeletal development to captive propagation, it is surprising that this information is not yet available for *S. ocellatus* or *C. nebulosus*. Despite the successful captive propagation programs that exist for both species throughout the United State and China (Hong and Zhang, 2003; Vega et al., 2009), the detailed information compiled on skeleton development herein should be of direct benefit to the future propagation of both species should skeletal malformations become an issue in the future. Additionally, having temporal data for skeletal development for both *S. ocellatus* and *C. nebulosus* may be useful for determining at which stage in the development of the skeleton (early, late, or inbetween) the bones that exhibit abnormalities develop in the sequence of normal skeletal development. In addition to the obvious advantages for captive propogation, detailed studies on skeletal development in additional species of teleosts can only further our understanding of skeletal development in this successful group of vertebrates.

CONCLUSIONS

Skeletal formation, excluding the basisphenoid and the sclerotics, was complete at 14.4 mm SL and 13.5 mm SL in *S. ocellatus* and *C. nebulosus* respectively. The basisphenoid appeared later in development for both species (21.9 mm SL in *S. ocellatus* and 19.5 mm SL in *C. nebulosus*) while the sclerotic were not present in any material examined, suggesting they appear at larger sizes than those examined. No major differences in the order of skeletal development were seen between the two species, although there were a few minor differences in the sequence of ossification. Variation was observed in two skeletal elements of *C. nebulosus*, the coronomekelian and supraneural 1. No major differences were observed when comparing the development of the axial skeleton of *Agyrosomus regius* to *S. ocellatus* and *C. nebulosus*, suggesting it may be conserved within sciaenidae. Several differences were noted when comparing the neurocranium development of *Micropogonias furnieri* to *S. ocellatus* and *C. nebulosus*, suggesting variation may exist in the development of the neurocranium within sciaenidae. Only four differences in the development of the skeleton were seen between *S. ocellatus* and *Danio rerio*, the only other teleost for which the complete ossification sequence is available, while 14 differences were identified when compared to *C. chanos*, for which the sequence of cranial development is available. This suggests variation exists between these three groups of fishes. This information will help contribute to the relatively small amount of information available on skeletal development of teleost fishes as well as provide information on the normal skeletal development of *S. ocellatus* and *C. nebulosus.* It will provide a standard reference sequence of skeletal development for both species that will facilitate identification of skeletal malformations should they become an issue in the future.

REFERENCES

Acha, E. M.; Mianzan, H.; Lasta, C. A.; Guerrero, R. A., 1999: Estuarine spawning of the whitemouth croaker *Micropogonias furnieri* (Pisces: Sciaenidae), in the Río de la Plata, Argentina. Mar. Freshwater Res. 50(1), 57-65.

Arratia, G.; Bagarinao, T., 2010: Early ossification and development of the cranium and paired girdles of *Chanos chanos* (Teleostei, Gonorynchiformes). In: Gonorynchiformes and Ostariophysan Relationships: a Comprehensive Review. Enfield, New Hampshire: Science Publishers, 73-106.

Bird, N. C.; Mabee, P. M., 2003: Developmental morphology of the axial skeleton of the zebrafish, *Danio rerio* (Ostariophysi: Cyprinidae). Dev. Dynam. 228(3), 337-357.

Blasina, G.; Barbini, S.; Díaz de Astarloa, J., 2010: Trophic ecology of the black drum, *Pogonias cromis* (Sciaenidae), in Mar Chiquita coastal lagoon (Argentina). J. Appl. Ichthyol. 26(4), 528-534.

Britz, R.; Conway, K., 2009: Osteology of *Paedocypris*, a miniature and highly developmentally truncated fish (Teleostei: Ostariophysi: Cyprinidae). J. Morphol. 270(4), 389-412.

Britz, R.; Johnson, G. D., 2002: "Paradox Lost": skeletal ontogeny of *Indostomus paradoxus* and its significance for the phylogenetic relationships of Indostomidae (Teleostei, Gasterosteiformes). American Museum Novitates 3383, 1-43.

Britz, R.; Johnson, G. D., 2005: Occipito-vertebral fusion in ocean sunfishes (Teleostei: Tetraodontiformes: Molidae) and its phylogenetic implications. J. Morphol. 266(1), 74-79.

Britz, R.; Johnson, G. D., 2012: Ontogeny and homology of the skeletal elements that form the sucking disc of remoras (Teleostei, Echeneoidei, Echeneidae). J. Morphol. 273(12), 1353-1366.

Cardeira, J.; Vallés, R.; Dionísio, G.; Estévez, A.; Gisbert, E.; Pousão-Ferreira, P.; Cancela, M.; Gavaia, P., 2012: Osteology of the axial and appendicular skeletons of the meagre *Argyrosomus regius* (Sciaenidae) and early skeletal development at two rearing facilities. J. Appl. Ichthyol. 28(3), 464-470.

Cubbage, C. C.; Mabee, P. M., 1996: Development of the cranium and paired fins in the zebrafish *Danio rerio* (Ostariophysi, Cyprinidae). J. Morphol. 229(2), 121-160.

Daniel, S. J., 2004: Investigations into the nutritional requirements of juvenile dusky kob, *Argyrosomus japonicus* (Pisces sciaendae), under ambient culture conditions. MSc Thesis, Rhodes University, Grahamstown, South Africa.

Faustino, M.; Power, D. M., 2001: Osteologic development of the viscerocranial skeleton in sea bream: alternative ossification strategies in teleost fish. J. Fish. Biol. 58(2), 537-572.

Food and Agriculture Organization of the United Nations, F. D., 2012: The State of World Fisheries and Aquaculture(FAO, Rome). FAO, Rome. Available at: http://www.fao.org/docrep/016/i2727e/i2727e00.htm

Fritzsche, R. A.; Johnson, G. D. 1980: Early osteological development of white perch and striped bass with emphasis on identification of their larvae. T. Am. Fish. Soc. 109(4), 387-406.

Fruge, D. J.; Truesdale, F. M., 1978: Comparative larval development of *Micropogon undulatus* and *Leiostomus xanthurus* (Pisces: Sciaenidae) from the northern Gulf of Mexico. Copeia 1978(4), 643-648.

Gavaia, P.; Dinis, M.; Cancela, M., 2002: Osteological development and abnormalities of the vertebral column and caudal skeleton in larval and juvenile stages of hatchery-reared Senegal sole (*Solea senegalensis*). Aquaculture 211(1), 305-323.

Green, M., 1941: The cranial and appendicular osteology of *Aplodinotus grunniens* Rafinesque. Transactions of the Kansas Academy of Science (1903-) 44, 400-413.

Holt, J.; Johnson, A. G.; Arnold, C.; Fable Jr, W.; Williams, T., 1981: Description of eggs and larvae of laboratory reared red drum, *Sciaenops ocellata*. Copeia 1981(4), 751-756.

Hong, W.; Zhang, Q., 2003: Review of captive bred species and fry production of marine fish in China. Aquaculture 227(1), 305-318.

Jardim, L. F. A.; Santos, F. K., 1994: Development of the neurocranium in *Micropogonias furnieri* (Perciformes: Sciaenidae). Jpn. J. Ichthyol. 41, 131-139.

Kengo Itagaki, M.; Hidekazu Ohikawara, M.; Ferraz Dias, J.; Katsuragawa, M., 2007: Description of larvae and juveniles of *Bairdiella ronchus* (Sciaenidae: Teleostei) in southeastern Brazil. Sci. Mar. 71(2), 249-257.

Koumoundouros, G., 2010: Morpho-anatomical abnormalities in Mediterranean marine aquaculture. In: Recent advances in aquaculture research, G. Koumoundouros (Ed.), Transworld Research Network, Kerala, India, 125–148.

Koumoundouros, G.; Divanach, P.; Kentouri, M., 2000: Development of the skull in *Dentex dentex* (Osteichthyes: Sparidae). Mar. Biol. 136(1), 175-184.

Koumoundouros, G.; Divanach, P.; Kentouri, M., 2001: Osteological development of *Dentex dentex* (Osteichthyes: Sparidae): dorsal, anal, paired fins and squamation. Mar. Biol. 138(2), 399-406.

Koumoundouros, G.; Gagliardi, F.; Divanach, P.; Boglione, C.; Cataudella, S.; Kentouri, M., 1997: Normal and abnormal osteological development of caudal fin in *Sparus aurata* L. fry. Aquaculture 149(3), 215-226.

Lewis-McCrea, L. M.; Lall, S. P., 2007: Effects of moderately oxidized dietary lipid and the role of vitamin E on the development of skeletal abnormalities in juvenile Atlantic halibut (*Hippoglossus hippoglossus*). Aquaculture 262(1), 142-155.

Li, P.; Burr, G. S.; Goff, J.; Whiteman, K. W.; Davis, K. B.; Vega, R. R.; Neill, W. H.; Gatlin, D. M., 2005: A preliminary study on the effects of dietary supplementation of brewers yeast and nucleotides, singularly or in combination, on juvenile red drum (*Sciaenops ocellatus*). Aquac. Res. 36(11), 1120-1127.

Neira, F. J.; Miskiewicz, A. G.; Trnski, T., 1998: Larvae of temperate Australian fishes: laboratory guide for larval fish identification. Nedlands: University of Western Austrailia Press.

Nelson, J. S., 2006: Fishes of the World. Hoboken, New Jersey: Wiley.

Ono, R. D.; Poss, S. G., 1982: Structure and innervation of the swim bladder musculature in the weakfish, *Cynoscion regalis* (Teleostei: Sciaenidae). Can. J. Zool. 60(8), 1955-1967.

Potthoff, T.; Kelley, S.; Javech, J. C., 1986: Cartilage and bone development in scombroid fishes. Fish. B-NOAA. 84(3), 647-678.

Potthoff, T.; Tellock, J. A., 1993: Osteological development of the snook, *Centropomus undecimalis* (Teleostei, Centropomidae). B. Mar. Sci. 52(2), 669-716.

Ramcharitar, J.; Gannon, D. P.; Popper, A. N., 2006: Bioacoustics of fishes of the family Sciaenidae (croakers and drums). T. Am. Fish. Soc. 135(5), 1409-1431.

Reiss, J. O., 1989: The meaning of developmental time: a metric for comparative embryology. Am. Nat. 134(2), 170-189.

Sasaki, K., 1989: Phylogeny of the family Sciaenidae, with notes on its zoogeography (Teleostei: Perciformes). Memoirs of the Faculty of Fisheries-Hokkaido University, 36.

Taniguchi, N., 1969a: Comparative osteology of the sciaenid fishes from Japan and its adjacent waters. I. Neurocranium. Jap. J. Ichthyol. 16(2), 15-27.

Taniguchi, N., 1969b: Comparative osteology of the sciaenid fishes from japan and its adjacent waters. II. Vertebrae. Jap. J. Ichthyol. 16(4), 153-156.

Taniguchi, N., 1970: Comparative osteology of the sciaenid fishes from Japan and its adjacent waters. III. Premaxillary and dentary. Jap. J. Ichthyol. 17, 135-140.

Taylor, W. R., 1967: An enzyme method of clearing and staining small vertebrates. Proc. US. Nat. Mus. 122, 1-17

Taylor, W. R.; Van Dyke, G., 1985: Revised procedures for staining and clearing small fishes and other vertebrates for bone and cartilage study. Cybium 9(2), 107-119.

Thomas, D. L., 1971: The early life history and ecology of six species of drums (Sciaenidae) in the Lower Delaware River: a brackish tidal estuary. Cornell University, Ithaca, New York.

Tong, X. H.; Liu, Q. H.; Xu, S. H.; Ma, D. Y.; Xiao, Z. Z.; Xiao, Y. S.; Li, J., 2012: Skeletal development and abnormalities of the vertebral column and of the fins in hatchery-reared turbot *Scophthalmus maximus*. J. Fish. Biol. 80(3), 486-502.

Topp, R. W.; Cole, C. F., 1968: An osteological study of the sciaenid genus, *Sciaenops* Gill (Teleostei, Sciaenidae). B. Mar. Sci. 18(4), 902-945.

Vega, R. R.; Neill, W. H.; Gold, J. R.; Ray, M. S., 2009: Enhancement of Texas sciaenids (red drum and spotted seatrout). Paper presented at the Interactions of fisheries and fishing communities related to aquaculture (R. Stickney, R. Iwamoto, and M. Rust, eds.). Proceedings of the Thirty-Eight US-Japan Aquaculture Panel Symposium, Corpus Christi, Texas.

Walker, M, B.; Kimmel, C. B., 2007: A two-color acid-free cartilage and bone stain for zebrafish larvae. Biotech. Histochem. 82(1), 23-28.

Weitzman, S. H., 1962: The osteology of *Brycon meeki*: a generalized characid fish, with an osteological definition of the family: Stanford University, Division of Systematic Biology.

Weitzman, S. H., 1974: Osteology and evolutionary relationships of the Sternoptychidae, with a new classification of stomiatoid families. Bull. Am. Mus. Nat. Hist. 153, 327-478.